Published in Marine Chemistry 211 (2019) 117–130

REE distribution and Nd isotope composition of estuarine waters and bulk sediment leachates tracing lithogenic inputs in eastern Canada

Marie Casse[1,2,§], Jean-Carlos Montero-Serrano[1,2, §,*], Guillaume St-Onge[1,2], André Poirier[2]

[1] Institut des sciences de la mer de Rimouski, Canada Research Chair in Marine Geology, Université du Québec à Rimouski, 310 allée des Ursulines, Rimouski, Québec, G5L 3A1, Canada

[2] GEOTOP Research Center, 201 Av. Président Kennedy, Montréal, Québec, Canada

[§] Authors contributed equally.

* Corresponding author: J.-C. Montero-Serrano, E-mail address: jeancarlos_monteroserrano@uqar.ca.

Abstract

The rare earth element (REE) concentrations and the neodymium (Nd) and strontium (Sr) isotope compositions of the detrital fraction and authigenic Fe–Mn oxyhydroxide coatings of marine sediments may provide valuable information for better understanding the pathways of weathering inputs and estuarine and coastal exchange processes on different time scales. Here, we present the REE concentrations and $^{143}Nd/^{144}Nd$ (expressed in epsilon units, εNd) and $^{87}Sr/^{86}Sr$ ratios of detrital and authigenic (leached Fe–Mn oxyhydroxides) fractions from sediment core-top samples and of estuarine water samples collected in the Estuary and Gulf of St. Lawrence (EGSL) and continental shelf off southeastern Canada. The REE distribution patterns, εNd values, and $^{87}Sr/^{86}Sr$ isotopic values from the detrital fraction allow for the discrimination of sediment from continental sources in the EGSL. Sediments in the Baie des Chaleurs and on the continental shelf, which have εNd values ranging from −14.3 to −16, $^{87}Sr/^{86}Sr$ values ranging from 0.72708 to 0.71475, and low La/Yb and Gd/Yb ratios, are mainly supplied by the early Paleozoic Appalachian Mountains. In contrast, sediments in the Laurentian and Esquiman channels (εNd = −18.7 to −21.8, $^{87}Sr/^{86}Sr$ = 0.72068 to 0.72607, and high La/Yb and Gd/Yb ratios) come from the Grenvillian metamorphic rocks in the

Canadian Shield, and surface sediments on the southern Labrador Shelf (εNd = −28.7, $^{87}Sr/^{86}Sr$= 0.73062, and high La/Yb and Gd/Yb ratios) mainly originate from the Hudson Strait and Baffin Bay. The εNd values obtained from estuarine water samples and bulk sediment leachates are unradiogenic, with values ranging between −18.9 and −21.7 and between −16.1 and −27.2, respectively. Based on these results and the dissolved REE concentrations, we speculate that salt-induced coagulation of colloidal matter, dissolution of lithogenic sediments from the adjacent continents (notably from the erosion of the Grenville Province on the North Shore), bottom scavenging within the nepheloid layer, and brine rejection during sea ice formation significantly influence the distribution of REEs and the authigenic εNd signal throughout the water column in the EGSL. Overall, our results both underscore the fact that caution must be exercised when interpreting authigenic εNd records due to bottom water-mass mixing in estuarine and coastal marine environments and highlight the potential of REE and Nd-Sr isotope compositions in investigating changes in sediment sources and transport pathways in the EGSL.

Keywords: Estuary and Gulf of St. Lawrence; Rare earth element; Neodymium isotopes; Strontium isotopes; Particle scavenging; Sediment provenance; Estuarine processes.

1. Introduction

Estuaries are the interface between rivers and the ocean, and in these environments, the distribution of dissolved and particulate trace elements, including rare earth elements (REEs), depends not only on the chemical composition of the source rocks (Taylor and McLennan, 1985) but also on the physical and chemical processes that take place within the estuary (e.g., Palmer and Elderfield, 1985; Goldstein and Jacobsen, 1988; Elderfield et al., 1990; Sholkovitz, 1993, 1995; Adebayo et al., 2018). Therefore, estuaries significantly influence the trace element input from rivers into coastal waters and ultimately into the open

ocean (Pourret and Tuduri, 2017). Due to their high charge and small ionic radius, dissolved REEs are particle-reactive elements that are efficiently removed in the estuarine zone (Sholkovitz, 1993, 1995; Rousseau et al., 2015). Much of the removal of REEs, in particular light REEs (LREEs; such as La and Nd), in river-estuarine systems occurs at low salinities (<6.6), reflecting REE scavenging by salt-induced coagulation of river-borne colloids and adsorption onto Fe-organic colloids and particulate organic carbon (Elderfield et al., 1990; Goldstein and Jacobsen, 1988; Sholkovitz, 1993, 1995; Sholkovitz and Szymezak, 2000; Rousseau et al., 2015; Merschel et al., 2017).

Among the REEs, neodymium (Nd) isotopes (denoted εNd, which reflects the $^{143}Nd/^{144}Nd$ ratio normalized to the chondritic uniform reservoir; Jacobsen and Wasserburg, 1980) are a sensitive tracer for water mass mixing in the open ocean given the Nd residence time in seawater on the order of 500–1000 years (Tachikawa et al., 2003) and the distinct dissolved Nd isotope compositions of the major water masses involved (e.g., Frank, 2002; Goldstein and Hemming, 2003; Jeandel et al., 2007; Lacan et al., 2012). Seawater displays regional εNd signatures derived primarily from riverine continental input, particle-dissolved exchange processes (a process commonly referred to as boundary exchange) and/or benthic Nd flux (e.g., Frank, 2002; Jeandel et al., 2007; Wilson et al., 2013; Jeandel, 2016; Abbott et al., 2016; Haley et al., 2017). It is possible to reconstruct past deep-water Nd isotope signatures in seawater by analyzing the authigenic fraction from marine sediments, such as ferromanganese (Fe–Mn) oxyhydroxide coatings (e.g., Rutberg et al., 2000; Piotrowski et al., 2004; Bayon et al., 2004; Gutjahr et al., 2007). The Nd isotope signatures from authigenic iron (Fe) and manganese (Mn) coatings directly reflect the composition of the seawater because dissolved trace elements are incorporated by coprecipitation processes during early burial in the top few centimeters of sediments (e.g., Haley et al., 2004; Gutjahr et al., 2007). Thus, it has been assumed that bottom-water Nd isotope signatures are equivalent to those

77 obtained from sediment pore water in the upper few centimeters (Abbott et al., 2016; Haley et
78 al., 2017). Under oxic to suboxic conditions, strontium (Sr) is also incorporated into Fe–Mn
79 oxyhydroxide coatings within the uppermost few centimeters of the seafloor (Haley et al.,
80 2004). The oceanic residence time of Sr in the water column (2.5 Ma) is much longer (Hodell
81 et al., 1990) than the global turnover time of the ocean (approximately 1500 yr; Broecker and
82 Peng, 1982). Consequently, the Sr isotope ratio of seawater has changed but is globally
83 homogeneous at any given time (with a modern value of $^{87}Sr/^{86}Sr$ = 0.70917; Palmer and
84 Elderfield, 1985; Henderson et al., 1994; El Meknassi et al., 2018). Thus, the Sr isotope
85 signals obtained from authigenic Fe–Mn oxyhydroxide coatings can help to assess the
86 presence or absence of detrital contributions in bulk sediment leachates (e.g., Gutjahr et al.,
87 2007; Molina-Kescher et al., 2014). Moreover, lithogenic Sr is very mobile during chemical
88 weathering and can be easily removed from continental source regions (e.g., Millot et al.,
89 2002; Stevenson et al., 2018). Consequently, variations in the $^{87}Sr/^{86}Sr$ ratio of detrital
90 sediments have been shown to be a powerful tool for identifying changes in continental
91 weathering regimes on different time scales (e.g., Frank, 2002; Meyer et al., 2011). Therefore,
92 the combined use of εNd and $^{87}Sr/^{86}Sr$ values from detrital sediment may help in the
93 investigation of changes in weathering regimes and sediment provenance over time (e.g.,
94 Meyer et al., 2011; Asahara et al., 2012; Molina-Kescher et al., 2014).
95 The Estuary and Gulf of St. Lawrence (EGSL) in eastern Canada (**Figure 1**) includes
96 very dynamic environments from a sedimentary and geochemical point of view. Indeed, the
97 EGSL is characterized by a large volume of continental runoff, strong stratification of water
98 masses (Koutitonsky and Bugden, 1991), seasonal sea ice cover (Galbraith et al., 2016), and
99 high modern sedimentation rates (up to 0.74 cm/yr; Smith and Schafer, 1999; St-Onge et al.,
100 2003; Thibodeau et al., 2013). However, the origin, mixing and propagation of detrital
101 sediments and the influence of the input of riverine particulate material on estuarine water

chemistry in the EGSL have been poorly documented (e.g., D'anglejan and Smith 1973; Yeats and Loring, 1991; Casse et al., 2017). Thus, assessment of the REE concentrations and Nd and Sr isotope compositions of marine sediments and estuarine waters from the EGSL may provide valuable information to better understand the sedimentary dynamics and estuarine exchange processes occurring within this cold temperate region.

In this context, we present new REE concentrations and Nd and Sr isotope compositions for detrital and authigenic (leached Fe–Mn oxyhydroxides) fractions from sediment core-tops and for estuarine water samples collected in the EGSL and continental shelf off southeastern Canada. These data were used to (1) identify different source areas and transport pathways of detrital material in eastern Canada, (2) assess the presence or absence of detrital contributions in the REE and Nd isotope signatures extracted from the bulk sediment leachates (authigenic signal), and (3) assess the potential influences of estuarine processes and the input of lithogenic riverine materials on the dissolved REE and εNd patterns of estuarine waters in the EGSL.

2. Environmental setting

2.1. Regional morphology and geological setting

The EGSL bathymetry is profoundly marked by the Laurentian Channel, a U-shaped submarine valley resulting from Quaternary glacial erosion (Piper et al., 1990; St-Onge et al., 2011). This dominant topographic feature (250–500 m deep) extends from the eastern Canadian continental shelf to the mouth of the Saguenay Fjord near Tadoussac (e.g., St-Onge et al., 2011). Two other U-shaped channels are also well defined in the northeastern gulf: the Anticosti and Esquiman channels (**Figure 1B**). Moreover, surface sediments in the EGSL are characterized by fine-grained sediments (notably fine silts) in the deep central parts of the Laurentian Channel and by coarser-grained sediments (gravel, sand and, in lesser proportions,

fine silt) in the slopes and adjacent shelves (Loring and Nota, 1973; St-Onge et al., 2003; Barletta et al., 2010; Pinet et al., 2011; Jaegle, 2015).

Two main geological provinces characterize southeastern Canada (**Figure 1A**): (1) the Canadian Shield in the northern part, typified by old silicate rocks (Paleo- to Mesoproterozoic granites and gneisses) from the Grenville and Makkovik provinces (Culshaw et al., 2000; Farmer et al., 2003), and (2) the Appalachian Province in the southern part, composed of Paleozoic sedimentary rocks (including shale, limestone, dolostone, and calcareous shale; Loring and Nota, 1973). In this latter province, Paleozoic carbonate rocks crop out mainly on Anticosti Island and the western Newfoundland coast (Loring and Nota, 1973; Ebbestad and Tapanila, 2005).

According to several mineralogical and geochemical studies from eastern Canada (e.g., Loring and Nota, 1973; Farmer et al., 2003; Jaegle, 2015; Casse et al., 2017), detrital sediments in the Gulf of St. Lawrence are mainly derived from the eastern part of the Appalachians (notably from the Canadian Maritime Provinces) and western Newfoundland coast, with the Grenvillian metamorphic rocks of the Canadian Shield on the North Shore being a secondary source. Conversely, in the lower St. Lawrence Estuary, detrital sediments mainly originate from the North Shore (Jaegle, 2015; Casse et al., 2017). Sedimentary inputs from the southern Labrador margin are derived mainly from the Grenville and Makkovic provinces as well as from the Hudson Strait and Baffin Bay (Farmer et al., 2003).

2.2. Hydrological setting

The eastern Canadian continental shelf is directly affected by the southward flow of the Labrador Current Water (LCW), a shelf-bathing water mass that reaches depths slightly greater than 600 m (Yashayaev et al., 2007). The LCW can be divided into 2 major branches (**Figure 1A**), outer and inner (Lazier and Wright, 1993; Yashayaev et al., 2007). The outer

LCW is composed of the West Greenland Current (WGC) and the Baffin Current (BC) and carries approximately 80% of the south-bound water, while the inner LCW is strongly influenced by outflow from the Hudson Strait that mixes with Baffin Bay water (Drinkwater, 1996; Lazier and Wright, 1993).

The EGSL is a transitional environment between the St. Lawrence River and the Northwest Atlantic Ocean (**Figure 1A**). Circulation in the EGSL is therefore estuarine, with a lower-salinity surface layer flowing seawards and saltier subsurface and bottom layers flowing landwards (Koutitonsky and Bugden, 1991): (1) the thin, seaward-flowing surface layer (down to 50 m) has a temperature of 2–10°C and a salinity of 25–32, and it originates from the mixing of seawater with freshwater runoff from the Great Lakes, the St. Lawrence River, and the northern Quebec drainage system; (2) a cold (−1 to 2°C) and saline (31.5–33) subsurface layer (50–150 m) forms from the winter cooling of dense surface waters as tributary flow decreases and ice forms; and (3) a warmer (3–6°C) and saltier (34–35) landward-flowing bottom layer (> 150 m deep) that originates from the edge of the continental shelf through mixing between cold, fresh, and oxygen-rich waters from the outer LCW and warm, salty, and oxygen-poor North Atlantic Central Water (NACW). In this bottom layer, the mixing proportion between the outer LCW and the NACW varies on a decadal or secular time scale (e.g., Bugden, 1991; Gilbert et al., 2005, 2007; Thibodeau et al., 2010). Indeed, Gilbert et al. (2005) suggested a change in the relative proportion of outer LCW and NACW in the water mass entering the Laurentian Channel from the 1930s to the 1980s. Based on instrument temperature and salinity measurements of the outer LCW and the NACW, these authors propose that the Laurentian Channel bottom waters were composed of approximately 72% LCW and 28% NACW in the 1930s and approximately 53% LCW and 47% NACW in the 1980s.

The annual mean circulation in the EGSL is principally characterized by coastal currents with dominantly E–W flow, such as the Gaspé Current, the Anticosti Gyre, and the inflowing West Newfoundland Current, which flows northward along the west coast of Newfoundland (**Figure 1B**). These currents are characterized by a mean speed on the order of ~1 cm/s (Tang, 1980). In the EGSL, one of the most striking features of near-surface circulation is the Gaspé Current, which is a buoyancy-driven coastal jet that originates in the St. Lawrence Estuary (near Rimouski), flows seaward along the coast of the Gaspé Peninsula (Sheng, 2001) and finally exits the gulf through the Cabot Strait. The tidal pulse from the Atlantic Ocean enters the Gulf of St. Lawrence from two directions, through the Cabot Strait and Strait of Belle Isle (**Figure 1B**). Water mass circulation through the Strait of Belle Isle is mainly characterized by a branch of the inner LCW that flows southwest along the Labrador coast into the Gulf of St. Lawrence (**Figure 1B)**. The Cabot Strait represents a direct connection between the EGSL and the Northwest Atlantic Ocean, where seawater masses passing through it are characterized by a mixture of the NACW and the outer LCW (Gilbert et al., 2005). Notably, in addition to tidal pulses from the Atlantic Ocean, internal tides and waves can also be responsible for sediment remobilization in the EGSL (e.g., Normandeau et al., 2014).

2.3. Sediment and seawater εNd and $^{87}Sr/^{86}Sr$ variations in eastern Canada and adjacent continental shelves

The lithogenic Nd isotopic signature of sediments from the eastern Canadian Shield shows that the glaciomarine sediments from the western basin of the Hudson Strait and Baffin Bay have very unradiogenic Nd isotope compositions (i.e., low $^{143}Nd/^{144}Nd$ ratios and εNd values) with εNd values ranging from −28 to −29 and −23 to −27, respectively (Piepgras and Wasseburg, 1987; Farmer et al., 2003; Rashid et al., 2012). The Precambrian crust of the

North American Shield is also characterized by a very unradiogenic εNd signature (εNd ≈ −36 to −45; Innocent et al., 1997; Rashid et al., 2012; Hollings et al., 2008). Sediments originating from the Grenville Province have an unradiogenic Nd isotope composition (εNd ≈ −22; Farmer et al., 2003; Pratte et al., 2017; **Figure 1A**) and a large range of $^{87}Sr/^{86}Sr$ signatures of 0.70982–0.77457 (Millot et al., 2002; Namur et al., 2010). The Appalachian Province in the southern part of the EGSL records a Panafrican Nd isotope signature (εNd ≈ −10 to −14; Hollings et al., 2008; Fagel and Hilaire Marcel, 2006; Phan et al., 2018; **Figure 1A)** and $^{87}Sr/^{86}Sr$ values of 0.71110–0.76329 (Portier, 2015; Vinciguerra et al., 2016; Phan et al. 2018). Overall, as εNd and $^{87}Sr/^{86}Sr$ vary widely according to the different geological provinces present in eastern Canada, we can use sediment εNd and $^{87}Sr/^{86}Sr$ signatures to reconstruct sediment provenance changes in the EGSL (e.g., Farmer et al., 2003).

In the eastern part of the Strait of Belle Isle and north of Newfoundland, the modern inner LCW has unradiogenic εNd values ranging from −26 to −23 (Piepgras and Wasserburg, 1987; Filippova et al., 2017), clearly documenting terrestrial inputs from the Precambrian terrains of the Canadian Shield (e.g., Farmer et al., 2003; Rashid et al., 2012). In contrast, the outer LCW is currently characterized by more radiogenic εNd compositions with mean values ranging between −15 and −14 around the tail of the Grand Banks of Newfoundland, likely reflecting mixing with water masses that have more radiogenic isotopic signatures, such as WGC, BC, the Irminger Current, and the North Atlantic Current (Lacan and Jeandel, 2004; Lacan et al., 2012; Filippova et al., 2017; **Figure 1A)**. Seawater from Baffin Bay exhibits very unradiogenic εNd values (−25), dominated by Archean sources (Stordal and Wasserburg, 1986). Conversely, the NACW (which originates in the temperate Northwest Atlantic) is characterized by the most radiogenic εNd values in the area, ranging from −11 to −9 (Tachikawa et al., 1999; Lacan et al., 2012; Lambelet et al., 2016; **Figure 1A)**.

3. Materials and Methods

A total of 12 core-top sediment samples were collected at different depths in the EGSL and adjacent continental shelves (**Figure 1; Table S1**) during several oceanographic missions on board the R/V Coriolis II (COR-05, -06, -09 and -10), the Marion Dufresne (MD-99) and the Canadian Coast Guard Ship Hudson (HU-2003). The sampling of the uppermost 1 cm of sediment (core-top) was performed using a box core, trigger weight core and/or piston core sampler (**Table S1**). The box core (BC) sampler is designed for recovering a relatively undisturbed sample of the sediment-water interface. Likewise, the trigger weight corer (TWC) collected in conjunction with a piston corer (PC) also allows recovery of the sediment-water interface, which is usually perturbed when the piston corer enters the sediments. Thus, the core-top (0-1 cm) sediments sampled with the BC and TWC are assumed to have recovered the sediment-water interface, while this may not necessarily be the case with the PC. Only core MD99-2236 was sampled with a long Calypso piston core system. Based on the fact that the modern sedimentation rates in the EGSL diminish exponentially from approximately 0.74 cm/yr at the head of the estuary to 0.15–0.20 cm/yr in the gulf to approximately 0.01 cm/yr at the mouth of the Laurentian Channel in the Atlantic (e.g., Smith and Schafer, 1999; Muzuka and Hillaire-Marcel, 1999; St-Onge et al., 2003; Barletta et al., 2010; Genovesi et al., 2011; Thibodeau et al., 2013), we can therefore estimate the these core-top sediment samples represent, on average, modern times or at least younger than the last 170 years, except for core MD99-2236, in which the core-top represents around 425 years according to Jennings et al. (2015). To compare the Nd isotopic data derived from the Fe–Mn oxyhydroxide coatings of sediment particles, 15 water samples from three different depths were recovered from 5 stations (COR1206-030, COR1206-025, COR1207-003, COR1207-007, and COR1503-007, hereinafter referred to as S1, S2, S3, S4, and S5, respectively) along the axis of the Laurentian Channel, from its head to its mouth, during the cruises COR1206, COR1207, and COR1503

of the R/V Coriolis II in the fall of 2012 and the summer of 2015 (**Figure 1B; Table S2**). Estuarine water samples were collected with a rosette equipped with 12 Niskin-type sample bottles and several Seabird sensors (conductivity, temperature, pressure, and beam transmission). The bottom water samples were collected in the benthic nepheloid layer (~10 m above the seafloor). The water samples were transferred into 20-L acid-cleaned LDPE collapsible cubitainers and stored in a cold room. All water samples were filtered in the laboratory using a 0.45 µm membrane (Millipore Corp.) and then acidified to a pH of ~2 with Suprapur 6 M HCl, following GEOTRACES recommendations (van de Flierdt et al., 2012).

Detailed descriptions of the methods are provided in the supplementary material. Briefly, the preconcentration of REEs of estuarine water was performed following the analytical procedures outlined in Shabani et al. (1992) and Jeandel et al. (1998). Nd and Sr isotope compositions from the authigenic Fe–Mn coatings of bulk sediment were extracted following the leaching protocol of Chen et al. (2012). The residual fraction remaining after leaching the bulk sediment (i.e., the detrital fraction) was digested using a hydrofluoric-nitric-perchloric (HF-HNO_3-$HClO_4$) procedure modified from Révillon and Hureau-Mazaudier (2009). Sr and Nd were separated from other elements using a single-step ion chromatographic separation process (Li et al., 2014). Subsequently, REE concentrations were determined using an inductively coupled plasma quadrupole mass spectrometer (ICP-QMS Agilent 7500c) at the *Institut des sciences de la mer de Rimouski* (ISMER, Canada). Sr isotope ratios ($^{88}Sr/^{86}Sr$) were measured in dynamic mode on a Thermo Scientific Triton Plus™ multicollector thermal ionization mass spectrometer (TIMS) at GEOTOP (Montreal, Canada). Finally, Nd isotope ratios ($^{143}Nd/^{144}Nd$) were analyzed on a Nu Instruments multicollector inductively coupled plasma mass spectrometer (MC-ICP-MS), also at GEOTOP.

The REE measurements were normalized to the Post-Archaean Australian Shale (PAAS, Pourmand et al., 2012). Hence, the subscript "n" indicates PAAS-normalized abundances. Based on several geochemical studies that addressed REE concentrations in authigenic phases and seawater (Haley et al., 2004; Molina-Kescher et al., 2014; Osborne et al., 2015; Laukert et al., 2017), we used the HREE/LREE ratio (Yb_n/Nd_n) to investigate the fractionation between HREEs and LREEs. Similar to the processes used in other sediment provenance studies (e.g., Armstrong-Altrin et al., 2013, 2016), in the detrital fraction, HREE versus LREE enrichment was quantified by (La/Yb)n, HREE versus MREE enrichment was quantified by (Gd/Yb)n, and the Eu anomaly was quantified as follows: $Eu/Eu^* = Eu_n/(Sm_n*Gd_n)^{1/2}$. Nd isotope ratios are expressed as follows: $\varepsilon Nd = ([(^{143}Nd/^{144}Nd)_{sample}/(^{143}Nd/^{144}Nd)_{CHUR}]-1)x10000$ (CHUR: chondritic uniform reservoir; Jacobsen and Wasserburg, 1980).

4. Results

4.1. Seawater physical properties

The potential temperature (θ), salinity, and potential density (σ_θ) of water masses from the five estuarine stations (S1, S2, S3, S4, and S5) studied here show similar hydrographic properties (**Figure 2A)**. In the surface layer, the five stations have a low salinity (28.2–31.5), a high temperature (3–9°C), and a low potential density (21.9–25.5 kg/m^3). The subsurface layer has salinity values of 31.5–33.0, cold temperatures of −1.0–2.5°C, and potential density values of 25.5–26.5 kg/m^3. The bottom layer exhibits the highest salinity (34–35), a high temperature (4.0–6.7°C), and a high potential density (27–28 kg/m^3).

In general, surface and bottom layers have lower beam transmission intensities (82–92%) than the subsurface layer (97–100%) (**Figure 2B**). Based on these data, nepheloid

298 layers were identified between 250 and 310 m in the lower St. Lawrence Estuary and between
299 420 and 500 m at station S5 in the gulf (**Figure 2B**).
300
301 **4.2. REE concentrations**
302 The PAAS-normalized REE fractionation patterns are shown in **Figures 3 and 4**. The
303 Nd concentrations from the detrital and bulk sediment leachates samples ranged from 16 to 34
304 μg/g and from 0.05 to 1.4 μg/g, respectively (**Tables S4 and S5**). The PAAS-normalized REE
305 patterns of the detrital sediment samples display patterns with moderate LREE enrichment,
306 slightly depleted to flat HREEs and significant positive Eu anomalies (Eu/Eu*>1.3; **Table S4;**
307 **Figure 3A**). These LREE-enriched patterns were also evidenced by high (La/Yb)n and
308 (Gd/Yb)n ratios (**Figure 5C; Table S4**). However, note that the sediments from the Labrador
309 Shelf (MD9922-36) have the highest LREE and MREE enrichment. Likewise, sediments
310 from the Laurentian and Esquiman channels have higher (La/Yb)n and (Gd/Yb)n ratios than
311 sediments from the shelf (**Figure 5C**). Moreover, the PAAS-normalized REE patterns of the
312 bulk sediment leachates from the EGSL reveal an MREE bulge-type pattern (**Figure 3B**),
313 with greater enrichment of MREEs than of HREEs and LREEs, which is a common pattern in
314 leachates and authigenic material supplied by rivers (Haley et al., 2004; Gutjahr et al., 2007;
315 Du et al., 2016; Abbott et al., 2016).
316 The PAAS-normalized REE patterns in most water samples from the EGSL display
317 patterns characterized by a pronounced negative Ce anomaly together with HREE enrichment
318 (**Figure 4**). The negative Ce anomaly is generally more pronounced in the most saline deeper
319 water samples than in the surface and subsurface samples or in the gulf samples. However,
320 some surface and subsurface water samples from stations S1 to S4 have relatively flat REE
321 patterns with little to no Ce anomaly. The dissolved LREE concentrations (represented in this
322 study by Nd) from all of the water stations in the EGSL show a decreasing trend with depth,

323 i.e., from 22 pmol/kg in the surface and subsurface waters to 2.5 pmol/kg in the most saline
324 bottom water samples (**Figure 6A and 7A; Table S6**). This decreasing trend in the LREE
325 concentrations is exactly opposite to the pattern observed in the open ocean, in which the
326 surface features lower concentrations than the bottom (e.g., Zhang and Nozaki, 1996). The
327 range of Nd concentrations in the analyzed water samples is comparable with previously
328 published values from estuarine and coastal waters with a similar salinity range (28 to 35) and
329 strong riverine influence (3 to 60 pmol/kg; Sholkovitz and Szymezak, 2000, Osborne et al.,
330 2014; van de Flierdt et al., 2016). Likewise, most of the dissolved $(HREE/LREE)_n$ profiles in
331 the EGSL (except station S3) show a decrease in the first 50 m and then an increasing trend
332 with depth (**Figure 6B**). The dissolved $(HREE/LREE)_n$ ratios of surface water samples also
333 show an increasing trend from the estuary to the gulf stations.
334
335 **4.3. Sr and Nd isotope signatures**
336 The Sr and Nd isotope data obtained from the detrital sediments, bulk sediment
337 leachates and estuarine water are provided in **Table S7**. The detrital sediment samples feature
338 $^{87}Sr/^{86}Sr$ values ranging between 0.71475 and 0.73062 (median 0.72351), which are higher
339 than the values of the other sample types here studied. Indeed, the $^{87}Sr/^{86}Sr$ values obtained
340 from the bulk sediment leachates and estuarine water samples range between 0.70975 and
341 0.70870 (median 0.70925) and between 0.70915 and 0.70937 (median 0.70921), respectively
342 (**Figure 5A**). These values are close to the modern values from the shelf and oceanic waters
343 (0.70917 ± 0.00002; El Meknassi et al., 2018).
344 The εNd values obtained from the detrital sediment samples (**Figures 5A-B and 8A;**
345 **Table S7**) range between −14.3 (Baie des Chaleurs) and −28.7 (southern Labrador Shelf).
346 The detrital εNd values from the estuary range between −18.7 and −21.8, whereas the detrital

εNd values from the mouth and the continental shelves are more radiogenic, with values ranging from −14.3 to −16.

Replicate εNd analyses of two bulk sediment leachate samples (COR0602-36PC and COR0503-CL04-36PC) yielded similar εNd values within analytical uncertainty (**Table S7**). This similarity indicates a robust level of reproducibility for the entire analytical procedure used in our study. Such reproducibility of εNd analyses in bulk sediment leachates indicates that variations of approximately 2 ε units could be considered significant. The εNd values of bulk sediment leachates from the EGSL range between −16.1 (Baie des Chaleurs) and −27.2 (southern Labrador Shelf) (**Figures 5A-B and 8B-C; Table S7**). Bulk sediment leachate samples from the lower estuary have more unradiogenic εNd values (approximately −20), whereas samples from the mouth and continental shelves have slightly more radiogenic εNd values (approximately −18). Furthermore, the εNd values from the bulk sediment leachates and the detrital fraction display a significant positive linear correlation (r=0.88; n=10; **Figure 8C**).

The εNd values obtained for the estuarine water mass range between −19 and −22 (**Figures 5A, 6C and 9; Table S6**). No significant differences in εNd values between the surface waters and the most saline bottom waters from the same stations are observed (**Figures 6C, 7B, and 9**). The most radiogenic εNd values are observed at stations closest to the South Shore (S2 and S4; εNd = −17 to −18), and the least radiogenic Nd isotope compositions are observed at stations closest to the North Shore and the gulf (S1, S3, and S5; εNd = −19 to −22).

5. Discussion

To assess the influence of the input of lithogenic riverine material on the estuarine water chemistry of the EGSL, we first discuss the detrital REE and Nd-Sr isotope patterns and

their implications for identifying different source areas and transport pathways of detrital material in eastern Canada. We then compare the authigenic REE concentrations and Nd-Sr isotope values extracted from the bulk sediment leachates with the values in the overlying water column and in the detrital fraction to identify the main phase extracted during the leaching process. Furthermore, we evaluate the potential influence of estuarine processes and terrestrial inputs on the REE distribution and εNd signals of the estuarine waters in the EGSL.

5.1. Detrital REE and Nd-Sr isotope patterns in surface sediments in eastern Canada: Tracing potential sediment sources

The PAAS-normalized REE patterns of detrital sediments can provide important clues about source-rock characteristics (e.g., Montero-Serrano et al., 2009; Armstrong-Altrin et al., 2013, 2016; Osborne et al., 2015). Indeed, the significant positive Eu anomalies (Eu/Eu*>1.3; **Table S4**) observed in our detrital fraction are characteristic of sediments derived mainly from felsic igneous/metamorphic sources (e.g., Bayon et al., 2015). The positive Eu anomaly is generally attributed to the tendency of europium to be preferentially incorporated into plagioclase (Weill and Drake, 1973). Several sedimentological and mineralogical studies (Loring and Nota, 1973; Jaegle, 2015; Casse et al., 2017) have suggested that modern sedimentary inputs in the EGSL are derived mainly from the Canadian Shield on the North Shore and are characterized by high proportions of plagioclase feldspar (32–65%), potassium feldspar (7–21%), and amphibole (1–7%) (Jaegle, 2015). Thus, the high input of plagioclase from the Canadian Shield to the EGSL could explain the positive Eu anomaly observed in the detrital fraction.

Furthermore, the $^{87}Sr/^{86}Sr$ values of detrital sediments from the EGSL are relatively radiogenic and range between 0.71475 and 0.73062 (**Figure 5A**). These values are consistent with the $^{87}Sr/^{86}Sr$ data from the Grenville Province (0.70982 to 0.77457; Millot, 2002; Namur

et al., 2010) and the Appalachian Mountains (0.71110 to 0.76329; Portier, 2015; Vinciguerra et al., 2016; Phan et al. 2018). However, as the $^{87}Sr/^{86}Sr$ values from the Grenville and Appalachian domains overlap, it is difficult to distinguish between these sources of sediment in the EGSL based only on Sr isotopes. Therefore, we combine (La/Yb)n and (Gd/Yb)n ratios with Sr and Nd isotopes to better track the origin of the sediment (**Figure 5**). The diagrams reveal two distinctive sedimentary sources: the Appalachian domain and the Canadian Shield (including the Grenville, Nain, and Makkovik provinces; **Figure 1**).

The surface sediment samples collected on the Canadian continental shelf (COR1002-27BC, COR1004-ECL-BC, 2003-033-030PC, and COR0503-CL03-35BC) and at Baie des Chaleurs (COR0902-16BC) have εNd values ranging between −14.3 and −16.0, high $^{87}Sr/^{86}Sr$ ratios ranging between 0.71475 and 0.72708, low (La/Yb)n values ranging from 0.95 to 1.19, and low (Gd/Yb)n values of 1.02 to 1.16 (**Figure 5**). Taking into consideration the εNd values of the Grenville Province (εNd ≈ −22; Farmer et al., 2003; Pratte et al., 2017) and the Appalachian Province (εNd ≈ −11; Fagel and Hilaire Marcel, 2006; Phan et al. 2018) and using a conservative binary mixing, we estimated that the Nd isotope composition of these samples is 61% from Appalachian sources and only 39% from the Grenville Province (**Figure 10**). Farmer et al. (2003) identified a similar range of εNd values in deglacial sediments from the Gulf of St. Lawrence. Based on coastal current patterns in the EGSL (Galbraith et al., 2016), we suggest that the Appalachian sediments observed in these surface sediment samples are mainly transported via the Gaspé Current (**Figure 1B**). This coastal current separates into two branches downstream of the tip of the Gaspé Peninsula; the southern branch flows over the Magdalen Shelf and along the coast of the Canadian Maritime Provinces, whereas the northern branch flows along the western edge of the Laurentian Channel (Trites, 1972; Sheng, 2001). Thus, the southern branch forms the main outflow of the gulf on the western side of Cabot Strait and may therefore transport Appalachian sediments from the South Shore and

Canadian Maritime Provinces to the gulf and then to the continental shelf off southeastern Canada through the Cabot Strait (Loring and Nota, 1973; Dufour and Ouellet, 2007; Casse et al., 2017).

The sediment samples from the Laurentian (COR0503-CL04-36PC, COR0503-14BC, COR0602-043BC, COR0602-045BC, COR0602-36PC) and Esquiman (COR1004-CE-BC) channels feature low εNd values (−18.7 to −21.8), high $^{87}Sr/^{86}Sr$ values (0.72068 to 0.72607), and relatively high (La/Yb)n and (Gd/Yb)n values (1.23 to 1.53 and from 1.28 to 1.39, respectively; **Figure 5**), which are characteristic of the Canadian Shield source rocks (Farmer et al., 2003; Pratte et al., 2017). The overall Nd signature of the Canadian Shield is difficult to assess because these terranes are very complex and vary greatly in age (1.8–3.8 Ga; Innocent et al., 1997). The Nd isotope ratios from terranes belonging to the Canadian Shield record unradiogenic εNd values of −35.9 to −22 (Revel et al., 1996; Innocent et al., 1997; Dickin, 2000; Rashid et al., 2012; Pratte et al., 2017). According to **Figure 10**, detrital sediments from the Laurentian and Esquiman channels are characterized by a mixed detrital source; in other words, they are mainly from the Grenville Province (86%) but feature a notable contribution from the Appalachian Mountains (14%). The sediment samples from the Esquiman Channel have higher $^{87}Sr/^{86}Sr$ values (up to 0.72607) than the sediment from the Laurentian Channel (**Figure 5A**), probably due to their proximity to the Strait of Belle Isle, which is influenced by the inner LCW (Petrie and Anderson, 1983). Because the inner LCW transport large amounts of dissolved and suspended particulate material with distinctive geochemical signatures from the Hudson Strait and the Labrador continental margin (Lacan and Jeandel, 2005), this current can influence the geochemical composition of the surface sediments in the Esquiman Channel. However, further investigations are needed to gain a more precise understanding of the sediment contributions from the Hudson Strait and Labrador continental margin to the Esquiman Channel.

447 Finally, the sediment sample from the southern Labrador Shelf (Cartwright Saddle;
448 MD99-2236) has an εNd value of −28.7, a $^{87}Sr/^{86}Sr$ value of 0.73062, a high (La/Yb)n value
449 (approximately 1.77), and a high (Gd/Yb)n value (approximately 1.46) (**Figure 5**). These Nd
450 and Sr isotope values are characteristic of the Hudson Strait and Baffin Bay sediments
451 (Farmer et al., 2003), which are characterized by unradiogenic εNd values (~ −28.1 to −28.9
452 and −23.1 to −27.2, respectively) and high $^{87}Sr/^{86}Sr$ values (0.72205 to 0.72619 and 0.72611
453 to 0.73600, respectively). These unradiogenic εNd values may be associated with increased
454 detrital Nd and Sr inputs to this area by the inner LCW, which ultimately delivers Nd and Sr
455 eroded from the eastern Canadian Shield (Farmer et al., 2003; Lambelet et al., 2016;
456 Filippova et al., 2017).
457
458 **5.2. REE and Sr isotope values of bulk sediment leachates: Fingerprint of the authigenic**
459 **Fe–Mn oxyhydroxide fraction**
460 The REE distributions and $^{87}Sr/^{86}Sr$ values obtained from bulk sediment leachates can
461 be used to demonstrate the absence of detrital contamination during the leaching process and,
462 thus, to indicate that the REE and Nd isotope signals extracted from bulk sediment samples
463 are derived entirely from seawater (e.g., Gutjahr et al., 2007; Molina-Kescher et al., 2014; Du
464 et al., 2016). The PAAS-normalized REE plot of the bulk sediment leachate data shows
465 significant MREE enrichment (**Figure 3B**), which is not present in the detrital sediment
466 samples (**Figure 3A**). This MREE-enriched pattern is typical of Fe–Mn oxyhydroxide and
467 riverine particulate leachates (e.g., Haley et al., 2004; Gutjahr et al., 2007; Du et al., 2016;
468 Abbott et al., 2016), suggesting that these phases were principally extracted from the bulk
469 sediment samples. Moreover, as local rivers in the EGSL clearly play a predominant role in
470 the input of REEs (Gaillardet et al., 2003), we hypothesize that the REE patterns leached from
471 bulk sediment samples likely represent a mixture of locally formed and pre-formed

472 continental Fe–Mn oxyhydroxides (e.g., Bayon et al., 2004; Poulton and Raiswell, 2005;
473 Kraft et al., 2013). Alternatively, the MREE enrichment observed in our bulk sediment
474 leachates could also be caused by the dissolution of phosphates, such as apatite (Hannigan
475 and Sholkovitz, 2001; Pourret and Tuduri, 2017). With the data currently available, we cannot
476 validate or reject this last hypothesis. However, apatite appears to be negligible in the
477 sediment samples from the main rivers that feed the EGSL (Jaegle, 2015) and marine
478 sediments from the Laurentian Channel (Casse et al., 2017), as suggested by its low
479 abundance (<0.1%) or absence in the quantitative phase analysis (X-ray powder diffraction
480 method developed by Eberl, 2003 and Eberl and Smith, 2009) of X-ray diffractograms of bulk
481 sediment samples (**Figure S1**). Likewise, the remineralization of organic compounds in
482 estuarine and coastal marine sediments could also explain (at least partly) the REE
483 distribution in the bulk sediment leachates (Bayon et al., 2014; Freslon et al., 2014). However,
484 even if organic matter dominated the MREE bulge-type pattern, the dissolution of organic
485 compounds during the leaching processes would lead to an REE pattern 10 times more
486 enriched than the PAAS abundances (e.g., Freslon et al., 2014). Because our sediment
487 leachates are not characterized by a similar REE enrichment, we propose that the sedimentary
488 organic matter fraction was not extracted in our bulk sediment leachates.

489 Further evidence of the authigenic origin of the REEs in the bulk sediment leachates
490 can be obtained from $^{87}Sr/^{86}Sr$ values (e.g., Haley and Polyak 2013). The $^{87}Sr/^{86}Sr$ values
491 obtained from the modern estuarine water samples and leachate sediment in the EGSL
492 (median of 0.70921) are close to the global seawater value (**Figure 5A**). The 2.4 Myr
493 residence time of Sr in seawater is far longer than the mixing time of the oceans (1500 years;
494 Broecker and Peng, 1982), causing a globally uniform $^{87}Sr/^{86}Sr$ value in seawater and modern
495 marine carbonates ($^{87}Sr/^{86}Sr \approx 0.70917$; El Meknassi et al., 2018). This observation is
496 especially relevant in the EGSL, where biogenic sources of carbonates are negligible (less

than 1%; Jaegle, 2015; Casse et al., 2017) and detrital sediments typically have higher $^{87}Sr/^{86}Sr$ values (0.70982 to 0.77457; Millot et al., 2002; Namur et al., 2010; Vinciguerra et al., 2016; Phan et al. 2018).

Overall, all of these results suggest that authigenic Fe–Mn oxyhydroxide coatings are the dominant phase extracted in our bulk sediment leachates and that detrital and sedimentary organic matter contamination during the leaching procedure is negligible.

5.3. Dissolved REE and Nd isotope signatures of estuarine waters from the EGSL: Estuarine processes and potential influence of lithogenic inputs

The REE patterns of most of our water samples show a typical PAAS-normalized seawater REE pattern, which is characterized by a pronounced negative Ce anomaly together with progressive enrichment of heavy REEs (**Figure 4**). This pattern is consistent with coastal waters and oceanic REE trends (e.g., Piepgras and Jacobsen, 1992; Rousseau et al., 2015; Filippova et al., 2017; Pourret and Tuduri, 2017). The negative Ce anomaly is attributable to the higher particle reactivity of Ce due to its specific redox properties and its oxidative state (IV) compared to the other trivalent REEs (Elderfield et al., 1990; Sholkovitz, 1993, 1995). As previously reported for estuarine mixing zones (e.g., Elderfield et al., 1990; Sholkovitz, 1993, 1995; Sholkovitz and Szymczak, 2000; Rousseau et al., 2015; Merschel et al., 2017; Pourret and Tuduri, 2017; Adebayo et al., 2018), the higher particle reactivity of Ce becomes amplified during salt-induced coagulation of colloids in estuaries and thus is responsible for the increase in the negative Ce anomaly with increasing salinity. Based on these considerations, we suggest that the decreasing trend observed in most of the dissolved LREE profiles (represented here by Nd) from the EGSL with depth and increasing salinity (**Figures 6A and 7A**) can be attributed to the coagulation of colloidal material (Sholkovitz, 1993, 1995; Sholkovitz and Szymczak, 2000). Similar interpretations of dissolved metal concentrations in

522 the St. Lawrence Estuary have been reported by Yeats and Loring (1991). Furthermore,
523 bottom waters in the EGSL are characterized by decreased beam transmission (**Figure 2B**),
524 which are typically associated with suspended particulates in benthic nepheloid layers (e.g.,
525 Wu et al., 2015; Crocket et al., 2018). Thus, the lower Nd concentrations (~2.5 pmol/kg) and
526 high (HREE/LREE)n ratios (>1) recorded in the near-bottom waters at each station may be
527 linked to enhanced scavenging within the bottom nepheloid layer, likely through continuous
528 adsorption of dissolved REEs onto Fe–Mn oxyhydroxide phases and/or any other detrital and
529 authigenic phases.

530 Some surface and subsurface estuarine water samples (notably, S1-4m, S1-65m, S2-
531 4m, S3-75m, S4-5m, S4-60m; **Figure 4**) have relatively flat REE patterns with little to no Ce
532 anomaly, suggesting a major influence of local river inputs and, therefore, an enhanced
533 release of river-borne particulate REEs (Pourret and Tuduri, 2017). In this context, we
534 examined the (HREE/LREE)n ratios versus εNd values to document the potential influence of
535 the lithogenic inputs on the estuarine water chemistry of the EGSL (e.g., Osborne et al., 2015;
536 Laukert et al., 2017). In the (HREE/LREE)n - εNd crossplot (**Figure 11**), the REE data from
537 detrital sediments fall in the mixed detrital zone, close to the Grenville [εNd ≈ −19 to −21 and
538 (HREE/LREE)n ≈ 0.4 to 0.7] and Appalachian [εNd ≈ −12 and (HREE/LREE)n ≈ 1.1]
539 signatures (Pratte et al., 2017; Phan et al. 2018). On the other hand, REE data from seawater
540 samples from the inner LCW (stations BIL; Filippova et al., 2017), Gulf Stream (Bermuda
541 Atlantic Time Series Station, BATS; van de Flierdt et al., 2012) and North East Atlantic Deep
542 Water (station HL08; Filippova et al., 2017) form a well-constrained linear trend, here
543 referred to as the seawater array. In general, most of the surface and subsurface estuarine
544 waters (excluding the samples S2-4m, S2-305m, S3-3m and all S5 water samples) and bulk
545 sediment leachate samples from the EGSL are close to their potential detrital sources. These
546 estuarine water samples were collected from within the lower St. Lawrence Estuary (**Figure**

547 **1B**), in which the surface waters are characterized by a high suspended particulate matter
548 content (up to 2.2 mg/L; Yeats et al., 1979; Larouche and Boyer-Villemaire, 2010). In
549 agreement with previous geochemical studies in estuarine mixing zones (Sholkovitz, 1993,
550 1995; Sholkovitz and Szymczak, 2000; Freslon et al., 2014; Rousseau et al., 2015; Osborne et
551 al., 2015; Merschel et al., 2017; Adebayo et al., 2018), we hypothesize that the
552 (HREE/LREE)n values close to 1 in the surface and subsurface estuarine waters from the
553 lower St. Lawrence Estuary may be the result of high rates of partial dissolution and release
554 of river-borne particulate REEs.

555 The (HREE/LREE)n - εNd crossplot also suggests that additional estuarine processes
556 involving the removal and addition of REEs may be of local importance in the EGSL. The
557 closest seawater station to Cabot Strait (S5) exhibited the highest (HREE/LREE)n value (> 2)
558 (**Figure 11**). This zone is characterized by a low suspended particulate matter content in the
559 surface waters (0.2 to 0.4 mg/L; Larouche and Boyer-Villemaire, 2010), reducing the
560 potential for partial dissolution of riverine particulate material (Rousseau et al., 2015). In the
561 gulf, these environmental conditions, in conjunction with increasing distance from the detrital
562 source and intense degradation of particulate organic matter in the water column (Mai-Thi et
563 al., 2017), may be responsible for the continuous preferential removal of LREEs over HREEs
564 from the dissolved load (e.g., Sholkovitz, 1993, 1995; Sholkovitz and Szymczak, 2000) and,
565 therefore, for the increase in the (HREE/LREE)n ratio. In addition, the S2-4m, S2-305m, and
566 S3-3m water samples exhibited intermediate (HREE/LREE)n values (1.4 to 1.7). These
567 stations are located in zones of important vertical mixing of water masses due to cyclonic
568 structures, the Anticosti Gyre and the Gaspé Current (Dufour and Ouellet, 2007; Galbraith et
569 al. 2016). Thus, the intermediate (HREE/LREE)n values recorded at stations S2 and S3 are
570 probably the result of a combination of estuarine processes involving the partial dissolution of

571 riverine detrital particles and remineralization of estuary sediments (e.g., Lawrence and
572 Kamber, 2006).

573 On the other hand, the vertical distribution of dissolved εNd at all estuarine stations
574 shows unradiogenic Nd isotope values throughout the entire water column (average εNd ~
575 −19.6 ± 1.2; **Figures 6C and 7B)**, and the values are similar to the εNd (±2σ) values of the
576 detrital and bulk sediment leachate samples (**Figure 9**). Because terrigenous suspended
577 particles have a short residence time of a few days within the St. Lawrence Estuary (Syvitski
578 et al., 1983; Lucotte et al. 1991) and the water depth in the EGSL is quite low (<500 m), we
579 hypothesize that rapid scavenging by the salt-induced coagulation of colloidal matter and
580 subsequent dissolution of the labile mineral phases influenced the εNd values in the water
581 column of the EGSL. Moreover, the EGSL is considered to be a subarctic region, with air
582 temperatures below zero degrees Celsius during the winter, allowing the formation of sea ice
583 (Saucier, 2003; de Vernal et al., 2011). Diagrams of the winter temperature and salinity data
584 from a station south of Anticosti Island (Galbraith, 2006) reveal that during winter, the upper
585 120 m of the water column is characterized by a high salinity (approximately 31.8) and near-
586 freezing temperatures (approximately −2°C) due to cooling and brine rejection during ice
587 formation. Thus, brine rejection during sea ice formation may also play a significant role in
588 the distribution of the relatively homogeneous Nd isotope values in EGSL seawater (Haley
589 and Polyak 2013). The flow from the surface to the bottom of the high-density brines may
590 homogenize the Nd isotope composition of the water column. Similar observations have been
591 reported by Porcelli et al. (2009), Haley and Polyak (2013) and Laukert et al. (2017) in the
592 Arctic Ocean.

593 In summary, although we acknowledge that the low spatial and vertical resolution of
594 our water sampling (five stations and three water samples per station) introduces some
595 uncertainties into our interpretations, we speculate that salt-induced coagulation of colloidal

596 matter, dissolution/scavenging of lithogenic particles and brine rejection during sea ice
597 formation significantly influence the distribution of REEs throughout the water column in the
598 EGSL.
599
600 **5.4. Nd isotope signatures of bulk sediment leachates and estuarine waters in the EGSL:**
601 **Quantifying lithogenic sources**
602 Along continental margins, the dissolved Nd load can be altered by processes such as
603 partial dissolution of river-borne particulate material (e.g., Frank, 2002; Goldstein and
604 Hemming, 2003; Jeandel et al., 2007; Pearce et al., 2013; Jeandel, 2016; Stewart et al., 2016),
605 submarine groundwater discharge (Molina-Kescher et al., 2018), and benthic exchange
606 processes (Abbott et al., 2016; Haley et al., 2017). Furthermore, most of the dissolved Nd
607 within the water column precipitates to form oxyhydroxides in estuarine sediments (Goldstein
608 and Jacobsen, 1988; Elderfield et al., 1990; Ingri et al., 2000; Rousseau et al., 2015). In the
609 EGSL, the overall high agreement between the εNd values from bulk sediment leachates and
610 their corresponding detrital εNd values (r=0.88; n=10; **Figures 8C and 9**) supports the idea
611 that variations in authigenic Nd isotopic compositions result mainly from changes in the
612 partial dissolution of riverine detrital particulate material derived from the Grenvillian and
613 Appalachian provinces. Note that sample inhomogeneity combined with unwanted chemical
614 extraction of other phases during sequential leaching may be the cause of the variability in the
615 εNd (±2σ) values in the bulk sediment leachates (e.g., Rutberg et al., 2000; Gutjahr et al.,
616 2007; Haley et al., 2008). Alternatively, the release of REEs from pore waters that are derived
617 from partial dissolution of bottom sediments could also contribute to the offset observed
618 between the εNd signal of surface leached sediments and detrital signatures (Abbott et al.,
619 2016; Haley et al., 2017).

620 Taking into consideration the detrital εNd endmember values of the Grenville
621 Province and Appalachian Province and assuming a conservative binary mixing, we estimate
622 that the εNd values of dissolved Nd in the estuarine water of the EGSL reflect a mixture of
623 approximately 74% Nd derived from the Canadian Shield and 26% Nd derived from the
624 Appalachian domain (**Figure 10**). These results are in agreement with other estimates from
625 EGSL sediments based on bulk mineralogical data, which show a dominance of the sediment
626 contributions from the North Shore in the EGSL (Jaegle, 2015). However, we cannot preclude
627 the possibility that the LCW/NACW εNd signatures also contribute to our authigenic εNd
628 signal (**Figure 9**). Given the high river discharges and detrital influence in the EGSL, we
629 hypothesize that the LCW/NACW signal recorded in the EGSL bottom sediments is masked
630 by the detrital εNd signatures of continental river inputs. Consequently, dissolved Nd inputs
631 from the EGSL to North Atlantic surface waters may thus contribute an unradiogenic Nd
632 isotopic composition to the NACW.

633 Furthermore, the authigenic εNd values obtained from surface sediment leachates
634 closest to the North Shore (COR0602-043BC, COR1004-CE-BC, COR0503-HONOI-14BC,
635 and COR0602-045BC) have an unradiogenic εNd signature that can be obtained by a mixture
636 of 83% Nd inputs from the Grenville Province and 17% Nd inputs from the Appalachian
637 domain (**Figure 10**). In contrast, the surface sediment leachates from the shelves (HU2003-
638 033-30PC, COR0503-CL03-35BC, COR1004-ECL-BC, COR0902-16BC, and COR1002-
639 27BC) have more radiogenic εNd values composed of approximately 64% Nd inputs derived
640 from the weathering of the Appalachian Province and 36% Nd inputs derived from the
641 Grenville domain (**Figure 10**). Therefore, the authigenic εNd values of the bulk sediment
642 leachates in the EGSL cannot be used to track water mass provenance and mixing but instead
643 reflect the composition of the surrounding continental margins. This interpretation is in
644 agreement with the consideration that dissolved water mass εNd signatures are set at the

continental margins, where they would not trace water mass mixing (e.g., Frank, 2002; Jeandel et al., 2007; Rousseau et al., 2015; Stewart et al., 2016).

6. Summary and conclusion

We determined the REE distributions and Nd and Sr isotope compositions on a set of surface marine sediments and at five hydrological stations in the EGSL and continental shelf off southeastern Canada. The (La/Yb)n and (Gd/Yb)n ratios and the εNd and $^{87}Sr/^{86}Sr$ isotope values of detrital sediments allowed the discrimination of continental sediment sources. Modern surface sediments from the continental shelf and Baie des Chaleurs have εNd values ranging from −14.3 to −16.0, $^{87}Sr/^{86}Sr$ values ranging from 0.72708 to 0.71475 and low (La/Yb)n and (Gd/Yb)n values mainly derived from the Appalachian domain. In contrast, surface sediments from the Laurentian-Esquiman channels [εNd = −18.7 to −21.8; $^{87}Sr/^{86}Sr$ = 0.72607 to 0.72068; high (La/Yb)n and (Gd/Yb)n] principally originate from the Grenville Province, and surface sediments from the southern Labrador Shelf [εNd = −28.7; $^{87}Sr/^{86}Sr$ = 0.73062; high (La/Yb)n and (Gd/Yb)n] are likely derived from the Hudson Strait and Baffin Bay. Furthermore, both the estuarine waters (εNd values ranging from −18.9 to −21.7) and the bulk sediment leachates (εNd values ranging from −16.1 to −27.2) have unradiogenic εNd values. The REE distributions and HREE/LREE - εNd crossplots suggest that the authigenic εNd signal recorded in the EGSL results mainly from the erosion and weathering of the unradiogenic continental shield, notably the Grenville Province in the Canadian Shield (εNd ≈ −22). Overall, both the dissolved REE concentrations and Nd isotope distributions suggest that the distribution of REEs throughout the water column in the EGSL is probably influenced by salt-induced coagulation of colloidal matter, dissolution of lithogenic sediments (notably from the erosion of the Grenville Province on the North Shore), bottom scavenging within the nepheloid layer, and brine rejection during sea ice formation.

Based on the comparison of the εNd values of leached and detrital core-top samples to those of bottom water samples, we hypothesize that the LCW/NACW signal recorded in the EGSL bottom sediments is masked by the lithogenic εNd signals derived from river input. Consequently, the Nd isotope compositions extracted from bulk sediment leachates from the EGSL mainly represent unradiogenic εNd detrital signals from the adjacent continents.

This study provides a basis for comparing downcore εNd, $^{87}Sr/^{86}Sr$, (La/Yb)n, and (Gd/Yb)n values preserved in the EGSL sedimentary records in order to reconstruct and document past variations in continental inputs and sediment dispersal related to climate changes, particularly during the last glacial cycle when sediment inputs would have been different from those of today due to the presence of the Laurentide Ice Sheet.

Acknowledgments

This research was funded by the *Fonds de recherche du Québec – Nature et technologies* (New university researchers start up program to J.-C. Montero-Serrano), ISMER excellence scholarships (M. Casse), and the Natural Sciences and Engineering Research Council of Canada (NSERC) through Discovery Grants to J.-C. Montero-Serrano and G. St-Onge. We thank the captain, crew, and scientists of the COR0503 and COR0602, COR0902, COR1002, and COR1004 campaigns on board the R/V Coriolis II. We also thank Quentin Beauvais (ISMER), Pascal Guillot (Québec-Océan) and Joël Chassé (IML) for their technical support and advice. Finally, thanks to: Christine Laurin, Thomas Barbour and American Journal Experts for reviewing the grammar; the three anonymous reviewers for their constructive reviews, which improve the quality of the manuscript; and Thomas Bianchi and Alexandra Rao for their editorial work. All analytical data presented are available electronically in the Supplementary Appendix (Tables S4 to S7).

References

Abbott, A. N., Haley, B. A., and McManus, J. (2016). The impact of sedimentary coatings on the diagenetic Nd flux. Earth Planet. Sci. Lett. 449, 217–227. doi: 10.1016/j.epsl.2016.06.001.

Adebayo, S.B., Cui, M., Hong, T., White, C.D., Martin, E.E., and Johannesson, K.H. (2018). Rare Earth Elements Geochemistry and Nd Isotopes in the Mississippi River and Gulf of Mexico Mixing Zone. Front. Mar. Sci. 5:166. doi: 10.3389/fmars.2018.00166

Armstrong-Altrin, J.S., Nagarajan, R., Madhavaraju, J., Rosalez-Hoz, L., Lee, Y.I., Balaram, V., Cruz-Martínez, A., & Avila-Ramírez, G. (2013). Geochemistry of the Jurassic and Upper Cretaceous shales from the Molango Region, Hidalgo, eastern Mexico: Implications for source-area weathering, provenance, and tectonic setting. *Comptes Rendus Geoscience, 345*(4), 185–202.

Armstrong-Altrin, J.S., Lee, Y.I., Kasper-Zubillaga, J.J., & Trejo-Ramírez, E. (2016). Mineralogy and geochemistry of sands along the Manzanillo and El Carrizal beach areas, southern Mexico: implications for palaeoweathering, provenance and tectonic setting: Geochemistry of Beach Sands from Southern Mexico. *Geological Journal*, 57, 1446–1461.

Asahara, Y., Takeuchi, F., Nagashima, K., Harada, N., Yamamoto, K., Oguri, K., & Tadai, O. (2012). Provenance of terrigenous detritus of the surface sediments in the Bering and Chukchi Seas as derived from Sr and Nd isotopes: Implications for recent climate change in the Arctic regions. *Deep Sea Research Part II: Topical Studies in Oceanography*, 61, 155–171. doi:10.1016/j.dsr2.2011.12.004

Barletta, F., St-Onge, G., Stoner, J.S., Lajeunesse, P., & Locat, J. (2010). A high-resolution Holocene paleomagnetic secular variation and relative paleointensity stack from eastern

719 Canada. *Earth and Planetary Science Letters, 298*(1), 162–174.
720 doi:10.1016/j.epsl.2010.07.038
721 Barrat, J.-A., Keller, F., Amosse´, J., Taylor, R.N., Nesbitt, R.W., Hirata, T. (1996).
722 Determination of rare earth elements in sixteen silicate reference samples by ICP-MS
723 after Tm addition and ion exchange separation. Geostand. Newsl. 20, 133– 139.
724 Bayon, G., German, C.R., Burton, K.W., Nesbitt, R.W., & Rogers, N. (2004). Sedimentary
725 Fe–Mn oxyhydroxides as paleoceanographic archives and the role of aeolian flux in
726 regulating oceanic dissolved REE. *Earth and Planetary Science Letters*, *224*(3), 477–
727 492. doi:10.1016/j.epsl.2004.05.033
728 Bayon, G., Henderson, G.M., Etoubleau, J., Caprais, J.-C., Ruffine, L., Marsset, T.,
729 Dennielou, B., Cauquil, E., Voisset, M., & Sultan, N. (2015). U-Th isotope constraints
730 on gas hydrate and pockmark dynamics at the Niger delta margin. *Marine Geology,*
731 370, 87–98. doi:10.1016/j.margeo.2015.10.012
732 Bugden, G. L. (1991). Changes in the temperature-salinity characteristics of the deeper
733 waters of the Gulf of St. Lawrence over the past several decades. *Can. Spec. Publ. Fish.*
734 *Aquat. Sci.,* 113, 139-147.
735 Broecker, W.S., Peng, T.-H. (1982). Tracers in the Sea. Lamont-Doherty Geological
736 Observatory, Palisades, NY, 1982, pp. 690.
737 Casse, M. (2018). Reconstitution de la variabilité naturelle climatique et océanographique
738 dans l'estuaire et le golfe du Saint-Laurent au cours des 10,000 dernières années. Thèse.
739 Rimouski, Québec, Université du Québec à Rimouski, Institut des sciences de la mer de
740 Rimouski, 285 p.
741 Casse, M., Montero-Serrano, J.-C., & St-Onge, G. (2017). Influence of the Laurentide Ice
742 Sheet and relative sea-level changes on sediment dynamics in the Estuary and Gulf of
743 St. Lawrence since the last deglaciation, *Boreas*. doi:10.1111/bor.12230

744 Chen, T.-Y., Frank, M., Haley, B.A., Gutjahr, M., & Spielhagen, R.F. (2012). Variations of
745 North Atlantic inflow to the central Arctic Ocean over the last 14 million years inferred
746 from hafnium and neodymium isotopes, *Earth and Planetary Science Letters,* 353, 82–
747 92. doi:10.1016/j.epsl.2012.08.012
748 Copard, K., Colin, C., Frank, N., Jeandel, C., Montero Serrano, J.-C., Reverdin, G., Ferron,
749 B., 2011. Nd isotopic composition of water masses and dilution of the Mediterranean
750 outflow along the South-West European margin. Geochem. Geophys. Geosyst. 12,
751 Q06020, http://dx.doi.org/10.1029/2011GC003529.
752 Crocket K.C., Hill E., Abell R.E., Johnson C., Gary S.F., Brand T. and Hathorne E.C (2018).
753 Rare Earth Element Distribution in the NE Atlantic: Evidence for Benthic Sources,
754 Longevity of the Seawater Signal, and Biogeochemical Cycling. Front. Mar. Sci. 5:147.
755 doi: 10.3389/fmars.2018.00147.
756 Culshaw, N., Brown, T., Reynolds, P.H., & Ketchum, J.W. (2000). Kanairiktok shear zone:
757 the boundary between the Paleoproterozoic Makkovik Province and the Archean Nain
758 Province, Labrador, Canada. *Canadian Journal of Earth Sciences, 37*(9), 1245–1257.
759 doi:10.1139/e00-035
760 D'Anglejan, B.F., Smith, E.C., 1973. Distribution, transport, and composition of suspended
761 matter in the St. Lawrence estuary. Canadian Journal of Earth Sciences 10, 1380–1396.
762 De Vernal, A., St-Onge, G., & Gilbert, D. (2011). Oceanography and Quaternary geology of
763 the St. Lawrence Estuary and the Saguenay Fjord. *IOP Conference Series: Earth and*
764 *Environmental Science, 14*(1), 012004. doi:10.1088/1755-1315/14/1/012004
765 Dickin, A. P. (2000). Crustal formation in the Grenville Province: Nd-isotope evidence.
766 *Canadian Journal of Earth Sciences*, *37*(2-3), 165–181.

767 Drinkwater, K.F. (1996). Climate and oceanographic variability in the Northwest Atlantic
768 during the 1980s and early-1990s. *Journal of Northwest Atlantic Fishery Science* 18,
769 77-97.
770 Du, J., Haley, B. A., & Mix, A. C. (2016). Neodymium isotopes in authigenic phases, bottom
771 waters and detrital sediments in the Gulf of Alaska and their implications for paleo-
772 circulation reconstruction. *Geochimica et Cosmochimica Acta*, *193*, 14–35.
773 Dufour, R. & Ouellet, P. (2007). Estuary and Gulf of St. Lawrence Marine Ecosystem
774 Overview and Assessment Report. *Canadian Technical Report of Fisheries and Aquatic*
775 *Sciences*, 112 pp.
776 Eberl, D. D. 2003. User Guide to RockJock-A Program for Determining Quantitative
777 Mineralogy from X-Ray Diffraction Data. US Geological Survey. Open-File Rep. 03-
778 78.
779 Eberl, D. D., and D. B. Smith. 2009. Mineralogy of soils from two continental-scale transects
780 across the United States and Canada and its relation to soil geochemistry and climate.
781 Applied Geochemistry, 24(8):1394–1404.
782 Ebbestad, J.O.R. & Tapanila, L. (2005). Non-predatory borings in Phanerotrema
783 (Gastropoda), Early Silurian, Anticosti Island, Québec, Canada. *Palaeogeography, Palaeoclimatology, Palaeoecology*, *221*(3), 325–341. doi:10.1016/j.palaeo.2005.03.003
784
785 Elderfield, H., Upstill-Goddard, R., & Sholkovitz, E. R. (1990). The rare earth elements in
786 rivers, estuaries, and coastal seas and their significance to the composition of ocean
787 waters. *Geochimica et Cosmochimica Acta*, *54*(4), 971–991.
788 Fagel, N., Innocent, C., Stevenson, R. K., & Hillaire-Marcel, C. (1999). Deep circulation
789 changes in the Labrador Sea since the Last Glacial Maximum: New constraints from
790 Sm-Nd data on sediments. *Paleoceanography*, *14*(6), 777–788.

791 Fagel, N., & Hillaire-Marcel, C. (2006). Glacial/interglacial instabilities of the Western
792 Boundary Under Current during the last 365 kyr from Sm/Nd ratios of the sedimentary
793 clay-size fractions at ODP site 646 (Labrador Sea). *Marine Geology*, *232*(1), 87–99.
794 Farmer, G. L., Barber, D., & Andrews, J. (2003). Provenance of Late Quaternary ice-proximal
795 sediments in the North Atlantic: Nd, Sr and Pb isotopic evidence. *Earth and Planetary*
796 *Science Letters*, *209*(1-2), 227–243.
797 Filippova, A., Frank, M., Kienast, M., Rickli, J., Hathorne, E., Yashayaev, I.M., & Pahnke, K.
798 (2017). Water mass circulation and weathering inputs in the Labrador Sea based on
799 coupled Hf–Nd isotope compositions and rare earth element distributions. *Geochimica*
800 *et Cosmochimica Acta, 199*, 164–184. doi:10.1016/j.gca.2016.11.024
801 Frank, M. (2002). Radiogenic isotopes: Tracers of past ocean circulation and erosional input.
802 *Reviews of Geophysics*, *40*(1).
803 Freslon, N., Bayon, G., Toucanne, S., Bermell, S., Bollinger, C., Chéron, S., Etoubleau, J.,
804 Germain, Y., Khripounoff, A., Ponzevera, E., Rouget, M.-L. (2014). Rare earth
805 elements and neodymium isotopes in sedimentary organic matter. *Geochimica et*
806 *Cosmochimica Acta, 140,* 177–198. doi:10.1016/j.gca.2014.05.016
807 Galbraith, P. S., Chasse, J., Caverhill, C., Nicot, P., Gilbert, D., Pettigrew, B., Lefaivre, D.,
808 Brickman, D., Devine, L. & Lafleur, C. (2016). Physical Oceanographic Conditions in
809 the Gulf of St. Lawrence in 2015. *DFO Canadian Science Advisory Secretariat*
810 *Research Document 2016/056*, 90 pp.
811 Galbraith, P.S. (2006). Winter water masses in the Gulf of St. Lawrence. Journal of
812 Geophysical Research: Oceans 111(6), C06022, https://doi.org/10.1029/2005JC003159.
813 Gaillardet J, Viers J, Dupre B (2003). Trace elements in river waters. In: Dreaver JI,
814 Holland HD, Turekian KK (eds) Treatise on geochemistry. Surface and
815 groundwater weathering and soils, vol 5. Elsevier-Pergamon, Oxford, pp 225–272.

816 Genovesi, L., de Vernal, A., Thibodeau, B., Hillaire-Marcel, C., Mucci, A., 2011. Recent
817 changes in bottom water oxygenation and temperature in the Gulf of St. Lawrence:
818 micropaleontological and geochemical evidence. Limnology and Oceanography 56,
819 1319–1329.
820 Gilbert, D., Sundby, B., Gobeil, C., Mucci, A., & Tremblay, G.-H. (2005). A seventy-two-
821 year record of diminishing deep-water oxygen in the St. Lawrence estuary: The
822 northwest Atlantic connection. *Limnology and Oceanography*, *50*(5), 1654–1666.
823 Gilbert, D., Chabot D., Archambault P., Rondeau B., & Hébert S. (2007). Appauvrissement
824 en oxygène dans les eaux profondes du Saint-Laurent marin: causes possibles et
825 impacts écologiques. *Le Naturaliste Canadien*, *131*, 67–75.
826 Goldstein, S. J., & Jacobsen, S. B. (1988). Rare earth elements in river waters. *Earth and*
827 *Planetary Science Letters*, *89*(1), 35–47.
828 Goldstein, S. L., & Hemming, S. R. (2003). Long-lived isotopic tracers in oceanography,
829 paleoceanography, and ice-sheet dynamics. *Treatise on Geochemistry*, *6*(6), 453–489.
830 Gutjahr, M., Frank, M., Stirling, C., Klemm, V., Vandeflierdt, T., & Halliday, A. (2007).
831 Reliable extraction of a deepwater trace metal isotope signal from Fe–Mn oxyhydroxide
832 coatings of marine sediments. *Chemical Geology*, *242*(3), 351–370.
833 doi:10.1016/j.chemgeo.2007.03.021
834 Haley, B.A., Du, J., Abbott, A.N. & McManus, J. (2017). The Impact of Benthic Processes on
835 Rare Earth Element and Neodymium Isotope Distributions in the Oceans. Front. Mar.
836 Sci. 4:426. doi: 10.3389/fmars.2017.00426
837 Haley, B.A., & Polyak, L., 2013. Pre-modern Arctic Ocean circulation from surface sediment
838 neodymium isotopes: Deep Arctic circulation from Nd isotopes. *Geophysical Research*
839 *Letters*, *40*(5), 893–897. doi:10.1002/grl.50188.

840 Haley, B.A., Frank, M., Spielhagen, R.F., & Fietzke, J. (2008). Radiogenic isotope record of
841 Arctic Ocean circulation and weathering inputs of the past 15 million years: ACEX Pb,
842 Sr, Nd isotope records. *Paleoceanography 23*(1). doi:10.1029/2007PA001486
843 Haley, B. A., Klinkhammer, G. P., & McManus, J. (2004). Rare earth elements in pore waters
844 of marine sediments. *Geochimica et Cosmochimica Acta*, *68*(6), 1265–1279.
845 Hannigan, R. E., & Sholkovitz, E. R. (2001). The development of middle rare earth element
846 enrichments in freshwaters: weathering of phosphate minerals. *Chemical Geology*,
847 *175*(3-4), 495–508.
848 Henderson, G.M., Martel, D.J., O'Nions, R.K., Shackleton, N.J. (1994). Evolution of
849 seawater $^{87}Sr^{86}Sr$ over the last 400 ka: the absence of glacial/interglacial cycles. *Earth*
850 *and Planetary Science Letters, 128*(3-4), 643–651. doi:10.1016/0012-821X(94)90176-7.
851 Hodell, D.A., Mead, G.A., & Mueller, P.A. (1990). Variation in the strontium isotopic
852 composition of seawater (8 Ma to present) : Implications for chemical weathering rates
853 and dissolved fluxes to the oceans. *Chemical Geology: Isotope Geoscience section,*
854 *80*(4), 291–307.
855 Hollings, P., Stevenson, R., Meng, X., & Hillaire-Marcel, C. (2008). Impact of melting of the
856 Laurentide Ice Sheet on sediments from the upper continental slope off southeastern
857 Canada: evidence from Sm-Nd isotopes. *Canadian Journal of Earth Sciences*, *45*(11),
858 1243–1252.
859 Ingri, J., Widerlund, A., Land, M., Gustafsson, Ö., Andersson, P., & Öhlander, B. (2000).
860 Temporal variations in the fractionation of the rare earth elements in a boreal river; the
861 role of colloidal particles. *Chemical Geology*, *166*(1-2), 23–45.
862 Innocent, C., Fagel, N., Stevenson, R. K., & Hillaire-Marcel, C. (1997). Sm-Nd signature of
863 modern and late Quaternary sediments from the northwest North Atlantic: Implications

for deep current changes since the Last Glacial Maximum. *Earth and Planetary Science Letters*, *146*(3-4), 607–625.

Jacobsen, S. B., & Wasserburg, G. J. (1980). Sm-Nd isotopic evolution of chondrites. *Earth and Planetary Science Letters*, *50*(1), 139–155.

Jaegle, M. (2015). Nature et origine des sédiments de surface de l'estuaire du Saint-Laurent. M.Sc. thesis, Université du Québec à Rimouski, 83 pp.

Jeandel, C., Thouron, D., & Fieux, M. (1998). Concentrations and isotopic compositions of neodymium in the eastern Indian Ocean and Indonesian straits. *Geochimica et Cosmochimica Acta*, *62*(15), 2597–2607.

Jeandel, C., Arsouze, T., Lacan, F., Techine, P., & Dutay, J. (2007). Isotopic Nd compositions and concentrations of the lithogenic inputs into the ocean: A compilation, with an emphasis on the margins. *Chemical Geology*, *239*(1-2), 156–164.

Jeandel, C. (2016). Overview of the Mechanisms That Could Explain the 'Boundary Exchange' at the Land–ocean Contact. Philosophical Transactions of the Royal Society A 374 (2081): 20150287. doi:10.1098/rsta.2015.0287

Jennings, A. E., J. T. Andrews, C. Pearce, L. Wilson, and S. Olfasdottir (2015). Detrital carbonate peaks on the Labrador Shelf, a 13 to 7 ka template for freshwater forcing from the Hudson Strait outlet of the Laurentide Ice Sheet into the subpolar gyre, Quat. Sci. Rev. 107, 62–80.

Koutitonsky V.G. & Bugden G.L. (1991). The physical oceanography of the Gulf of St. Lawrence: a review with emphasis on the synoptic variability of the motion. *Can. Spec. Publ. Fish. Aquat. Sci.,* 113, 57-90.

Kraft, S., Frank, M., Hathorne, E.C., & Weldeab, S. (2013). Assessment of seawater Nd isotope signatures extracted from foraminiferal shells and authigenic phases of Gulf of Guinea sediments. *Geochimica et Cosmochimica Acta 121*, 414–435.

889 Lacan, F. & Jeandel, C. (2001). Tracing Papua New Guinea imprint on the central Equatorial
890 Pacific Ocean using neodymium isotopic compositions and Rare Earth Element
891 patterns. *Earth and Planetary Science Letters, 186*(3), 497–512. doi:10.1016/S0012-
892 821X(01)00263-1
893 Lacan, F., & Jeandel, C. (2004). Neodymium isotopic composition and rare earth element
894 concentrations in the deep and intermediate Nordic Seas: Constraints on the Iceland
895 Scotland Overflow Water signature: Iceland Scotland Overflow Water. *Geochemistry,*
896 *Geophysics, Geosystems*, *5*(11).
897 Lacan, F., & Jeandel, C. (2005). Acquisition of the neodymium isotopic composition of the
898 North Atlantic Deep Water: Neodymium Isotopic Composition. *Geochemistry,*
899 *Geophysics, Geosystems 6*(12). doi:10.1029/2005GC000956
900 Lacan, F., Tachikawa, K., & Jeandel, C. (2012). Neodymium isotopic composition of the
901 oceans: A compilation of seawater data. *Chemical Geology*, *300*, 177–184.
902 Lambelet, M., van de Flierdt, T., Crocket, K., Rehkämper, M., Kreissig, K., Coles, B.,
903 Rijkenberg, M.J.A., Gerringa, L.J.A., de Baar, H.J.W., & Steinfeldt, R. (2016).
904 Neodymium isotopic composition and concentration in the western North Atlantic
905 Ocean: Results from the GEOTRACES GA02 section. *Geochimica et Cosmochimica*
906 *Acta 177*, 1–29. doi:10.1016/j.gca.2015.12.019
907 Lawrence, M. G., and Kamber, B. S. (2006). The behaviour of the rare earth elements during
908 estuarine mixing-revisited. Mar. Chem. 100, 147–161. doi:
909 10.1016/j.marchem.2005.11.007
910 Larouche, P., and Boyer-Villemaire, U., 2010. Suspended particulate matter in the St.
911 Lawrence estuary and Gulf surface layer and development of a remote sensing
912 algorithm. Estuarine, Coastal and Shelf Science 90, 241-249.

913 Laukert, G., Frank, M., Bauch, D., Hathorne, E. C., Gutjahr, M., Janout, M., et al. (2017).
914 Transport and transformation of riverine neodymium isotope and rare earth element
915 signatures in high latitude estuaries: a case study from the Laptev Sea. Earth Planet. Sci.
916 Lett. 477, 205–217.
917 Lazier J.R.N. and Wright D.G. (1993). Annual velocity variations in the Labrador Current.
918 Journal of Physical Oceanography 23, 659–678.
919 Li, C.-F., Guo, J.-H., Yang, Y.-H., Chu, Z.-Y., & Wang, X.-C. (2014). Single-step separation
920 scheme and high-precision isotopic ratios analysis of Sr–Nd–Hf in silicate materials.
921 *Journal of Analytical Atomic Spectrometry*, *29*(8), 1467.
922 Loring, D. H., & Nota, D. J. G. (1973). Morphology and sediments of the Gulf of St.
923 Lawrence. *Bulletin of the Fisheries Research Board of Canada, 182*, 147 pp.
924 Lucotte, M., Hillaire-Marcel, C., Louchouarn, P., 1991. First-order organic-carbon budget in
925 the St-Lawrence lower estuary from C-13 data. Estuarine, Coastal and Shelf Science 32,
926 297-312.
927 Mai-Thi, N.-N., St-Onge, G., Tremblay, L. (2017). Contrasting fates of organic matter in
928 locations having different organic matter inputs and bottom water O2 concentrations.
929 Estuarine, Coastal and Shelf Science 198, 63-72.
930 Merschel, G., Bau, M., and Dantas, E. L. (2017). Contrasting impact of organic and inorganic
931 nanoparticles and colloids on the behavior of particle-reactive elements in tropical
932 estuaries: an experimental study. Geochim. Cosmochim. Acta 197, 1–13.
933 Meyer, I., Davies, G.R., & Stuut, J.-B.W. (2011). Grain size control on Sr-Nd isotope
934 provenance studies and impact on paleoclimate reconstructions: An example from deep-
935 sea sediments offshore NW Africa: Grain size control on Sr-Nd isotope. *Geochemistry,*
936 *Geophysics, Geosystems 12*(3). doi:10.1029/2010GC003355

937 Millot, R., Gaillardet, J., Dupré, B., & Allègre, C. J. (2002). The global control of silicate
938 weathering rates and the coupling with physical erosion: new insights from rivers of the
939 Canadian Shield. *Earth and Planetary Science Letters*, *196*(1), 83–98.
940 Molina-Kescher, M., Frank, M., & Hathorne, E. C. (2014). Nd and Sr isotope compositions of
941 different phases of surface sediments in the South Pacific: Extraction of seawater
942 signatures, boundary exchange, and detrital/dust provenance. *Geochemistry,*
943 *Geophysics, Geosystems*, *15*(9), 3502–3520.
944 Molina-Kescher, M., Hathorne, E. C., Osborne, A. H., Behrens, M. K., Kölling, M., Pahnke,
945 Frank, M., (2018). The influence of basaltic islands on the Oceanic REE distribution: A
946 case study from the Tropical South Pacific. Front. Mar. Sci., 5.
947 http://dx.doi.org/10.3389/fmars.2018.00050.
948 Montero-Serrano, J.C., Bout-Roumazeilles, V., Tribovillard, N., Sionneau, T., Riboulleau, A.,
949 Bory, A., & Flower, B. (2009). Sedimentary evidence of deglacial megafloods in the
950 northern Gulf of Mexico (Pigmy Basin). *Quaternary Science Reviews, 28*(27), 3333–
951 3347.
952 Muzuka, A.N.N., Hillaire-Marcel, C. (1999). Burial rates of organic matter along the eastern
953 Canadian margin and stable isotope constraints on its origin and diagenetic evolution.
954 *Marine Geology* 160, 251-270.
955 Namur O., Charlier, B., Toplis, M. J., Higgins, M. D., Liégeois, J.-P., Auwera, J. V. (2010).
956 Crystallization Sequence and Magma Chamber Processes in the Ferrobasaltic Sept Iles
957 Layered Intrusion, Canada. *Journal of Petrology* 51-6, 1203–1236,
958 https://doi.org/10.1093/petrology/egq016.
959 Normandeau, A., Lajeunesse, P., St-Onge, G., Bourgault, D., Drouin, S.S.-O., Senneville, S.,
960 & Bélanger, S. (2014). Morphodynamics in sediment-starved inner-shelf submarine

961 canyons (Lower St. Lawrence Estuary, Eastern Canada). *Marine Geology, 357*, 243–
962 255.
963 Osborne, A.H., Haley, B.A., Hathorne, E.C., Plancherel, Y., & Frank, M. (2015). Rare earth
964 element distribution in Caribbean seawater: Continental inputs versus lateral transport
965 of distinct REE compositions in subsurface water masses. *Marine Chemistry 177*, 172–
966 183.
967 Palmer, M.R., & Elderfield, H., (1985). Sr isotope composition of sea water over the past 75
968 Myr. *Nature, 314*(6011), 526–528. doi:10.1038/314526a0
969 Pearce, C. R., Jones,M. T., Oelkers, E. H., Pradoux, C., and Jeandel, C. (2013). The effect of
970 particulate dissolution on the neodymium(Nd) isotope and Rare Earth Element (REE)
971 composition of seawater. Earth and Planetary Science Letters 369, 138–147.
972 Petrie, B., & Anderson, C. (1983). Circulation on the newfoundland continental shelf.
973 *Atmosphere-Ocean, 21*(2), 207–226. doi:10.1080/07055900.1983.9649165
974 Piepgras, D. J., & Wasserburg, G. J. (1987). Rare earth element transport in the western North
975 Atlantic inferred from Nd isotopic observations. *Geochimica et Cosmochimica Acta*,
976 *51*(5), 1257–1271.
977 Piepgras, D.J., & Jacobsen, S.B. (1992). The behavior of rare earth elements in seawater:
978 Precise determination of variations in the North Pacific water column. *Geochimica et*
979 *Cosmochimica Acta, 56*(5), 1851–1862.
980 Pinet, N., Brake, V., Campbell, C., & Duchesne, M. (2011). Seafloor and Shallow Subsurface
981 of the St. Lawrence River Estuary. *Geoscience Canada, 38*(1).
982 Piotrowski, J.A., Larsen, N.K., & Junge, F.W. (2004). Reflections on soft subglacial beds as a
983 mosaic of deforming and stable spots. *Quaternary Science Reviews, 23*(9), 993–1000.
984 doi:10.1016/j.quascirev.2004.01.006

985 Piper, D. J. W., Mudie, P. J., Fader, G. B., Josenhans, H. W., MacLean, B., & Vilks, G.
986 (1990). Quaternary geology. In Keen, M. J. & Williams, G. L. (eds.): Geology of the
987 Continental Margin of Eastern Canada, 475–607. Geology of Canada, Series 2.
988 *Geological Survey of Canada*, Ottawa ON.
989 Phan, T.T., Gardiner, J.B., Capo, R.C., Stewart, B.W. (2018).Geochemical and multi-isotopic
990 (87Sr/86Sr, 143Nd/144Nd, 238U/235U) perspectives of sediment sources, depositional
991 conditions, and diagenesis of the Marcellus Shale, Appalachian Basin,
992 USA.Geochimica et Cosmochimica Acta 222, 187-211.
993 Porcelli, D., Andersson, P.S., Baskaran, M., Frank, M., Björk, G., & Semiletov, I. (2009). The
994 distribution of neodymium isotopes in Arctic Ocean basins. *Geochimica et*
995 *Cosmochimica Acta, 73*(9), 2645–2659. doi:10.1016/j.gca.2008.11.046
996 Portier, A.M. (2015). Sediment provenance in the Gulf of Mexico: a test of the regolith
997 hypothesis. Master thesis, University of Florida, 66 p.
998 Poulton S. W. and Raiswell R. (2005). Chemical and physical characteristics of iron oxides in
999 riverine and glacial meltwater sediments. Chem. Geol. 218, 203–221.
1000 Pourmand, A., Dauphas, N., & Ireland, T.J. (2012). A novel extraction chromatography and
1001 MC-ICP-MS technique for rapid analysis of REE, Sc and Y: Revising CI-chondrite and
1002 Post-Archean Australian Shale (PAAS) abundances. *Chemical Geology 291*, 38–54.
1003 Pourret, O., Tuduri, J., 2017. Continental shelves as potential resource of rare earth elements.
1004 Scientific Reports, 7, 5857, DOI:10.1038/s41598-017-06380-z.
1005 Pratte, S., De Vleeschouwer, F., & Garneau, M. (2017). Geochemical characterization (REE,
1006 Nd and Pb isotopes) of atmospheric mineral dust deposited in two maritime peat bogs
1007 from the St. Lawrence North Shore (eastern Canada). *Journal of Quaternary Science*,
1008 *32*, 617–627.

1009 Rashid, H., F. Saint-Ange, D. C. Barber, M. E. Smith, and N. Devalia (2012). Fine scale
1010 sediment structure and geochemical signature between eastern and western North
1011 Atlantic during Heinrich events 1 and 2. Quat. Sci. Rev. 46, 136–150.
1012 Revel, M., Sinko, J.A., Grousset, F.E., & Biscaye, P.E. (1996). Sr and Nd isotopes as tracers
1013 of North Atlantic lithic particles: Paleoclimatic implications. *Paleoceanography, 11*(1),
1014 95–113. doi:10.1029/95PA03199
1015 Révillon, S., and D. Hureau-Mazaudier, 2009. Improvements in digestion protocols for trace
1016 element and isotope determinations in stream and lake sediment reference materials
1017 (JSd-1, JSd-2, JSd-3, JLk-1 and LKSD-1). Geostandards & Geoanalytical Research 33,
1018 397-413.
1019 Rousseau, T. C., Sonke, J. E., Chmeleff, J., Van Beek, P., Souhaut, M., Boaventura, G., et al.
1020 (2015). Rapid neodymium release to marine waters from lithogenic sediments in the
1021 Amazon estuary. Nature Communications 6:7592. doi: 10.1038/ncomms8592.
1022 Rutberg, R. L., Hemming, S. R., & Goldstein, S. L. (2000). Reduced North Atlantic Deep
1023 Water flux to the glacial Southern Ocean inferred from neodymium isotope ratios.
1024 Nature 405, 935-938.
1025 Samson, S.D., Barr, S.M., & White, C.E. (2000). Nd isotopic characteristics of terranes within
1026 the Avalon Zone, southern New Brunswick. *Canadian Journal of Earth Sciences, 37*(7),
1027 1039–1052. doi:10.1139/e00-015
1028 Saucier, F.J. (2003). Modeling the formation and circulation processes of water masses and
1029 sea ice in the Gulf of St. Lawrence, Canada. *Journal of Geophysical Research, 108*(C8).
1030 doi:10.1029/2000JC000686
1031 Schlitzer, R., 2017. Ocean data view. http://odv.awi.de.
1032 Shabani, M. B., Akagi, T., & Masuda, A. (1992). Preconcentration of trace rare-earth
1033 elements in seawater by complexation with bis (2-ethylhexyl) hydrogen phosphate

and 2-ethylhexyl dihydrogen phosphate adsorbed on a C18 cartridge and determination by inductively coupled plasma mass spectrometry. *Analytical Chemistry*, *64*(7), 737–743.

Sheng, J. (2001). Dynamics of a buoyancy-driven coastal jet: The Gaspe Current. *Journal of Physical Oceanography*, *31*(11), 3146–3162.

Sholkovitz, E.R. (1993). The geochemistry of rare-earth elements in the Amazon River estuary. Geochim. Cosmochim. Acta 57, 2181–2190.

Sholkovitz, E. R. (1995). The aquatic chemistry of rare earth elements in rivers and estuaries. Aquatic Geochemistry 1, 1–34. doi: 10.1007/BF01025229.

Sholkovitz, E., & Szymczak, R., (2000). The estuarine chemistry of rare earth elements: comparison of the Amazon, Fly, Sepik and the Gulf of Papua systems. *Earth and Planetary Science Letters, 179*(2), 299–309. doi:10.1016/S0012-821X(00)00112-6

Spivack, A. J., & Wasserburg, G. (1988). Neodymium isotopic composition of the Mediterranean outflow and the eastern North Atlantic. *Geochimica et Cosmochimica Acta*, *52*(12), 2767–2773.

Smirnova, E.V., Fedorova, I.N., Sandimirova, G.P., Petrov, L.L., Balbekina, N.G., Lozhkin, V.I., 2003. Determination of rare earth elements in black shales by inductively coupled plasma mass spectrometry. Spectrochim. Acta B: Atomic Spectroscopy 58, 329-340.

Smith, J.N., Schafer, C.T., 1999. Sedimentation, bioturbation, and Hg uptake in the sediments of the estuary and Gulf of St. Lawrence. Limnology and Oceanography 44, 207–219.

Stevenson, R., Pearce, C.R., Rosa, E., Hélie, J.-F., Hillaire-Marcel, C. (2018). Weathering processes, catchment geology and river management impacts on radiogenic (87Sr/86Sr) and stable (δ88/86Sr) strontium isotope compositions of Canadian boreal rivers. Chemical Geology 486, 50-60.

1059 Stewart, J.A., Gutjahr, M., James, R.H., Anand, P., Wilson, P.A. (2016). Influence of the
1060 Amazon River on the Nd isotope composition of deep water in the western equatorial
1061 Atlantic during the Oligocene–Miocene transition. Earth and Planetary Science Letters
1062 454, 132-141.
1063 St-Onge, G., Stoner, J.S., & Hillaire-Marcel, C. (2003). Holocene paleomagnetic records from
1064 the St. Lawrence Estuary, eastern Canada: centennial- to millennial-scale geomagnetic
1065 modulation of cosmogenic isotopes. *Earth and Planetary Science Letters, 209*(1-2),
1066 113–130.
1067 St-Onge, G., Duchesne, M. J., & Lajeunesse, P. (2011). Marine geology of the St. Lawrence
1068 Estuary. *IOP Conference Series: Earth and Environmental Science*, *14*, 012003.
1069 Stordal, M. C., & Wasserburg, G. J. (1986). Neodymium isotopic study of Baffin Bay water:
1070 sources of REE from very old terranes. *Earth and Planetary Science Letters*, *77*(3),
1071 259–272.
1072 Syvitski, J.P.M., Silverberg, N., Ouellet, G., and Asprey, K.W., (1983). First observations of
1073 benthos and seston from a submersible in the lower St. Lawrence Estuary: Géographie
1074 physique et Quaternaire, v. 37, p. 227-240.
1075 Tachikawa, K. (2003). Neodymium budget in the modern ocean and paleo-oceanographic
1076 implications. *Journal of Geophysical Research*, *108*(C8).
1077 Tachikawa, K., Jeandel, C., Vangriesheim, A., & Dupré, B. (1999). Distribution of rare earth
1078 elements and neodymium isotopes in suspended particles of the tropical Atlantic Ocean
1079 (EUMELI site). *Deep Sea Research Part I: Oceanographic Research Papers 46*(5),
1080 733–755.
1081 Tanaka, T., Togashi, S., Kamioka, H., Amakawa, H., Kagami, H., Hamamoto, T., Yuhara, M.,
1082 Orihashi, Y., Yoneda, S., Shimizu, H., Kunimaru, T., Takahashi, K., Yanagi, T.,
1083 Nakano, T., Fujimaki, H., Shinjo, R., Asahara, Y., Tanimizu, M., & Dragusanu, C.

(2000). JNdi-1: a neodymium isotopic reference in consistency with LaJolla neodymium. *Chemical Geology, 168*(3), 279–281.

Tang, C. L. (1980). Mixing and circulation in the northwestern Gulf of St. Lawrence: A study of a buoyancy-driven current system. *Journal of Geophysical Research*, *85*(C5), 2787.

Taylor S. R., and McLennan S.M. (1985). The continental crust: its composition and evolution. Blackwell Scientific Publication, Carlton, 312 p.

Thibodeau, B., De Vernal, A., Hillaire-Marcel, C., & Mucci, A. (2010). Twentieth century warming in deep waters of the Gulf of St. Lawrence: A unique feature of the last millennium: St. Lawrence Deep Waters Warming. *Geophysical Research Letters*, *37*(17).

Trites, R. W. (1972). The Gulf of St. Lawrence from a pollution point of view. In Ruivo, M. (ed.): Marine Pollution and Sea Life, 59–72. FAO Fishing News Books, London.

van de Flierdt, T., Griffiths, A.M., Lambelet, M., Little, S.H., Stichel, T., & Wilson, D.J. (2016). Neodymium in the oceans: a global database, a regional comparison and implications for palaeoceanographic research. *Philosophical Transactions of the Royal Society A: Mathematical, Physical and Engineering Sciences, 374*(2081), 20150293. doi:10.1098/rsta.2015.0293

van de Flierdt, T., Pahnke, K., Amakawa, H., Andersson, P., Basak, C., Coles, B., Colin, C., Crocket, K., Frank, M., Frank, N., Goldstein, S.L., Goswami, V., Haley, B.A., Hathorne, E.C., Hemming, S.R., Henderson, G.M., Jeandel, C., Jones, K., Kreissig, K., Lacan, F., Lambelet, M., Martin, E.E., Newkirk, D.R., Obata, H., Pena, L., Piotrowski, A.M., Pradoux, C., Scher, H.D., Schöberg, H., Singh, S.K., Stichel, T., Tazoe, H., Vance, D., & Yang, J. (2012). GEOTRACES intercalibration of neodymium isotopes and rare earth element concentrations in seawater and suspended particles. Part 1: reproducibility of results for the international intercomparison: Intercalibration of

Seawater Nd Isotopes. *Limnology and Oceanography: Methods 10*(4), 234–251. doi:10.4319/lom.2012.10.234

Vinciguerra, V., Stevenson, R., Pedneault, K., Poirier, A., Hélie, J.-F., & Widory, D. (2016). Strontium isotope characterization of wines from Quebec, Canada. *Food Chemistry*, *210*, 121–128.

Weill, D.F., & Drake, M.J. (1973). Europium Anomaly in Plagioclase Feldspar: Experimental Results and Semiquantitative Model. *Science 180*(4090), 1059–1060. doi:10.1126/science.180.4090.1059

Weis, D., Kieffer, B., Maerschalk, C., Barling, J., de Jong, J., Williams, G.A., Hanano, D., Pretorius, W., Mattielli, N., Scoates, J.S., Goolaerts, A., Friedman, R.M., & Mahoney, J.B. (2006). High-precision isotopic characterization of USGS reference materials by TIMS and MC-ICP-MS: isotopic study of USGS reference materials. *Geochemistry, Geophysics, Geosystems 7*(8). doi:10.1029/2006GC001283

Whalen, J.B., Jenner, G.A., Longstaffe, F.J., Robert, F., & GariéPy, C. (1996). Geochemical and Isotopic (O, Nd, Pb and Sr) Constraints on A-type Granite Petrogenesis Based on the Topsails Igneous Suite, Newfoundland Appalachians. *Journal of Petrology 37*(6), 1463–1489. doi:10.1093/petrology/37.6.1463

Wilson, D.J., Piotrowski, A.M., Galy, A., & Clegg, J.A. (2013). Reactivity of neodymium carriers in deep sea sediments: Implications for boundary exchange and paleoceanography. *Geochimica et Cosmochimica Acta, 109*, 197–221. doi:10.1016/j.gca.2013.01.042

Wu, Q., Colin, C., Liu, Z., Thil, F., Dubois-Dauphin, Q., Frank, N., Tachikawa, K., Bordier, L., & Douville, E. (2015). Neodymium isotopic composition in foraminifera and authigenic phases of the South China Sea sediments: Implications for the hydrology of the North Pacific Ocean over the past 25 kyr: hydrology of the North Pacific Ocean.

Geochemistry, Geophysics, Geosystems, 16(11), 3883–3904. doi:10.1002/2015GC005871

Yashayaev, I., M. Bersch, and H. M. van Aken (2007). Spreading of the Labrador Sea Water to the Irminger and Iceland basins. Geophys. Res. Lett., 34, L10602, doi:10.1029/2006GL028999

Yeats, P.A., and Loring, D.H. (1991). Dissolved and particulate metal distributions in the St. Lawrence estuary. Canadian Journal of Earth Sciences 28, 729-742.

Yeats, P.A., Sundby, B., & Bewers, J.M. (1979). Manganese recycling in coastal waters. Marine Chemistry, 8(1), 43–55.

Zhang J. and Nozaki Y. (1996). Rare earth elements and yttrium in seawater: ICP-MS determinations in the East Caroline, Coral Sea, and South Fiji basins of the western South Pacific Ocean. *Geochimica et Cosmochimica Acta* 60, 4631–4644.

Figure captions

Figure 1. (A) General map of the EGSL representing the location of the different core-top sediments analyzed in this study. The continental geological provinces are illustrated according to Farmer et al. (2003) with the εNd values of the Labrador Current Water (εNd ≈ −25; Piepgras and Wasserburg, 1987; Filippova et al., 2017) and North Atlantic Current Water (εNd ≈ −10; Spivack and Wasserburg, 1988; Lacan et al., 2012). (B) Simplified surface circulation models from the EGSL (modified from Galbraith et al. 2016) from October to December (gray vectors) and from April to June (red vectors). The locations of the different estuarine water stations studied here are also shown.

Figure 2. (A) Potential temperature (°C) versus salinity plot with potential density isopycnals (solid gray lines; σ_θ = potential density at reference pressure 0 m) for the five seawater stations analyzed in this study. Three distinctive sea water layers can be distinguished: a surface layer, a cold and saline subsurface layer, and a warmer and saltier bottom layer. This diagram was constructed using the ODV software (Schlitzer, 2017). (B) Vertical distribution of beam transmission data (% light attenuation) measured at the five estuarine water stations in the EGSL. BNL: benthic nepheloid layer.

Figure 3. (A) REE patterns normalized to PAAS for the detrital sediment samples. (B) REE patterns normalized to PAAS for the leachate sediment samples.

Figure 4. REE patterns normalized to PAAS at different depths at the five estuarine water stations. The PAAS-normalized REE patterns in most water samples from the EGSL display a pronounced negative Ce anomaly and enrichment in the heavy REEs.

Figure 5. Comparison of detrital sediment sample sources: (A) εNd versus $^{87}Sr/^{86}Sr$, (B) εNd versus (La/Yb)n, and (C) (La/Yb)n versus (Gd/Yb)n. The subscript "n" indicates PAAS-normalized abundances (Pourmand et al., 2012). Sediment samples from Baffin Bay, the western Hudson Strait, the southern Labrador Shelf, and the Gulf of St. Lawrence are also included (Fagel et al., 1999; Farmer et al., 2003). These three different detrital provinces are illustrated in colored arrays (gray, blue and orange).

Figure 6. Vertical distribution of (A) Nd concentrations, (B) PAAS-normalized HREE/LREE ratios, and (C) εNd values obtained from the five estuarine water stations. For a better

illustration of the data distribution, a logarithmic scale for Nd concentrations is used. Error bars represent the external 2-sigma errors.

Figure 7. Scatter plots of salinity versus (A) Nd concentration and (B) εNd values for the five estuarine water stations. For a better illustration of the data distribution, a logarithmic scale for Nd concentrations is used. In (B), the blue lines represent the mean (bold line; −19.6) and the standard deviation (dashed line; ±1.2) of all of the εNd data. The salinity versus Nd concentration plot shows a decreasing trend, while the salinity versus εNd plot does not exhibit significant differences between the surface waters and the most saline bottom waters from the same stations.

Figure 8. Spatial distribution of εNd values obtained from the (A) detrital surface sediments and (B) bulk sediment leachates. (C) εNd values of bulk sediment leachates versus those of detrital sediments. The external 2-sigma errors are represented by the symbol size. The blue line corresponds to the 1:1 slope. Larger differences between those two fractions ($\Delta\varepsilon Nd > 3$) are likely due to sample heterogeneity combined with unwanted chemical extraction of other phases during sequential leaching. (D) Vertical profiles of εNd values obtained from estuarine waters, bulk sediment leachates, and detrital sediments are shown. Seawater samples from the inner LCW (station BIL; Filippova et al., 2017) and the Western North Atlantic Central Water (WNACW; typified by the Bermuda Atlantic Time Series Station BATS-15m and Stn. 15; van de Flierdt et al., 2012; Lambelet et al., 2016) are also included. The Nd isotopic compositions of the bulk sediment leachates and estuarine waters in the EGSL mainly reflect the unradiogenic εNd signature of the Canadian Shield ($\varepsilon Nd \approx -22$ to -18). Error bars represent the external 2-sigma errors.

Figure 9. Relative contribution of the Appalachian source vs. the North American Shield. The relative percentages were calculated with the Nd isotope composition from the North American Shield ($^{143}Nd/^{144}Nd$ = 0.51105; Innocent et al., 1997) and Appalachian sources ($^{143}Nd/^{144}Nd$ = 0.512045; Fagel and Hilaire Marcel, 2006) according to $^{143}Nd/^{144}Nd_{(\%Grenville-Prov)}=[[(^{143}Nd/^{144}Nd_{sample}) - (0.512045-0.51105)]/ (0.512045-0.51105)]*100$.

Figure 10. (HREE/LREE)n - εNd crossplot including the detrital sediments, bulk sediment leachates and the estuarine waters analyzed in this study. Detrital sediments from the Grenville (Pratte et al., 2017) and Appalachian (Phan et al. 2018) provinces are shown. Seawater samples from the inner LCW (stations BIL; Filippova et al., 2017), the Western North Atlantic Central Water (Bermuda Atlantic Time Series Station BATS-15m; van de Flierdt et al., 2012) and the North East Atlantic Deep Water (NEADW; station HL08; Filippova et al., 2017) are also included.

Appendix A. Supplementary material

Supplementary material related to this article can be found online at http://dx.doi.org/XXXX

Supplementary table captions

Table S1. Location of core-top (0-1 cm) sediment samples with the corresponding water depth. Note that the box core (BC) sampler is designed for recovering a relatively undisturbed sample of the sediment-water interface. Likewise, the trigger weight corer (TWC) collected in conjunction with a piston corer (PC) also allows recovery of the sediment-water interface, which is usually perturbed when the piston corer enters the sediments. Thus, the core-top sediments sampled with the BC and TWC are assumed to have recovered the sediment-water

interface, while this may not necessarily be the case with the PC. Core-top sediment samples represent <170 years (Smith and Schafer, 1999; Muzuka and Hillaire-Marcel, 1999; St-Onge et al., 2003; Barletta et al., 2010; Genovesi et al., 2011; Thibodeau et al., 2013), except for core MD99-2236 where the core-top represents around 425 years (Jennings et al., 2015).

Table S2. Location of estuarine water samples together with the hydrological parameters. The potential temperature (θ °C), salinity, potential density (σ_θ) and beam transmission (% light attenuation) obtained from the five estuarine water stations S1 (COR1206-030), S2 (COR1206-025), S3 (COR1207-003), S4 (COR1207-007) and S5 (COR1503-07) are indicated.

Table S3. Analytical results of REE concentrations (CLMS-1 in ng/mL and BHVO-2 in μg/g) of certified reference materials determined by ICP-Q-MS. RD: relative deviation to reference values; RSD: relative standard deviation (1σ).

Table S4. REE concentrations (μg/g) for the detrital sediment samples. The HREE/LREE (Yb_n/Nd_n), (La/Yb)n, (Gd/Yb)n and Eu/Eu* ratios are also shown. The subscript "n" indicates the PAAS-normalized abundances (Pourmand et al., 2012).

Table S5. REE concentrations (ng/g) for the bulk sediment leachate samples. The HREE/LREE (Yb_n/Nd_n) ratios are also shown. The subscript "n" indicates PAAS-normalized abundances (Pourmand et al., 2012).

Table S6. REE concentrations from the five seawater stations (pmol/kg). The HREE/LREE (Yb_n/Nd_n) ratios are also shown. The subscript "n" indicates PAAS-normalized abundances (Pourmand et al., 2012).

Table S7. Neodymium (Nd) and strontium (Sr) isotope compositions obtained for the five estuarine water stations, bulk sediment leachates and detrital sediments. Note that the five water stations COR1206-030, COR1206-025, COR1207-003, COR1207-007 and COR1503-007 studied here are referred to as S1, S2, S3, S4, and S5, respectively. The symbols * and + indicate replicate analysis and NA indicate sample not analyzed.

Supplementary figure captions

Figure S1. Comparison between the X-ray diffractograms of four representative sediment samples from the EGSL (data are from Casse, 2018) with the apatite standard used in the XRD analysis (Eberl, 2003). Note that apatite was not detected (detection limit 0.1%; Eberl, 2003) in the X-ray diffractograms of the bulk sediments from the Laurentian Channel.

Figure 1

(Double column-full page width)

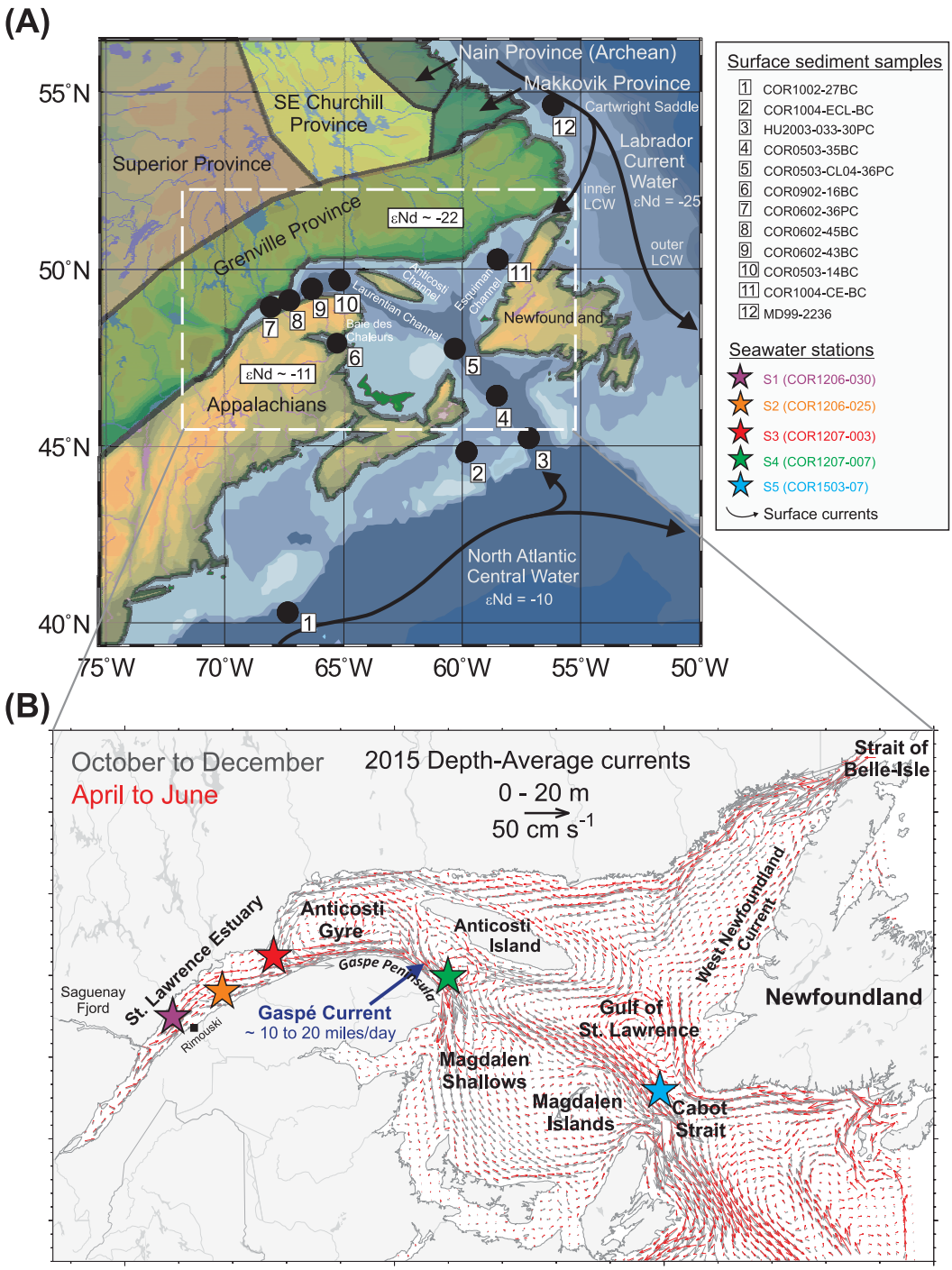

Figure 2

(Double column-full page width)

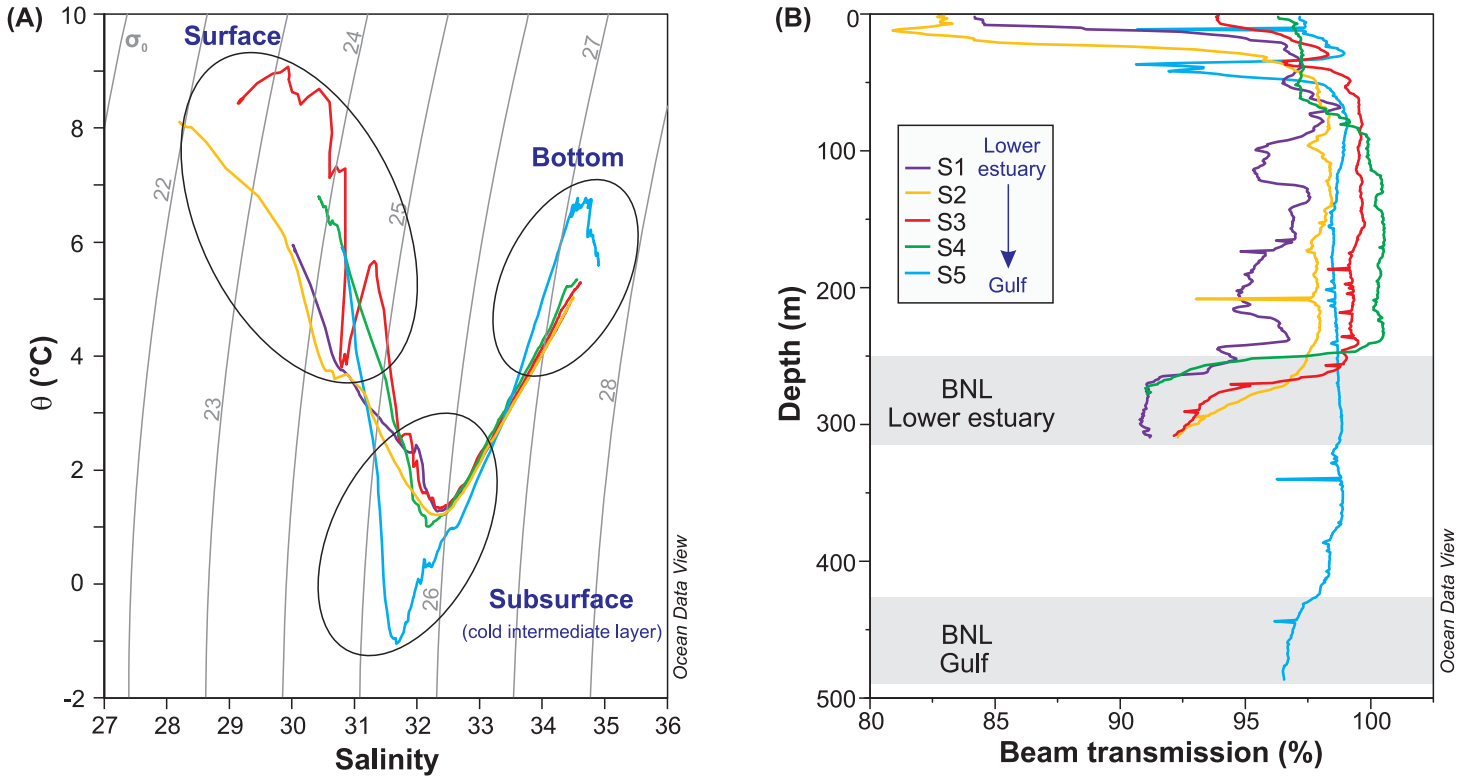

Figure 3

(Double column-full page width)

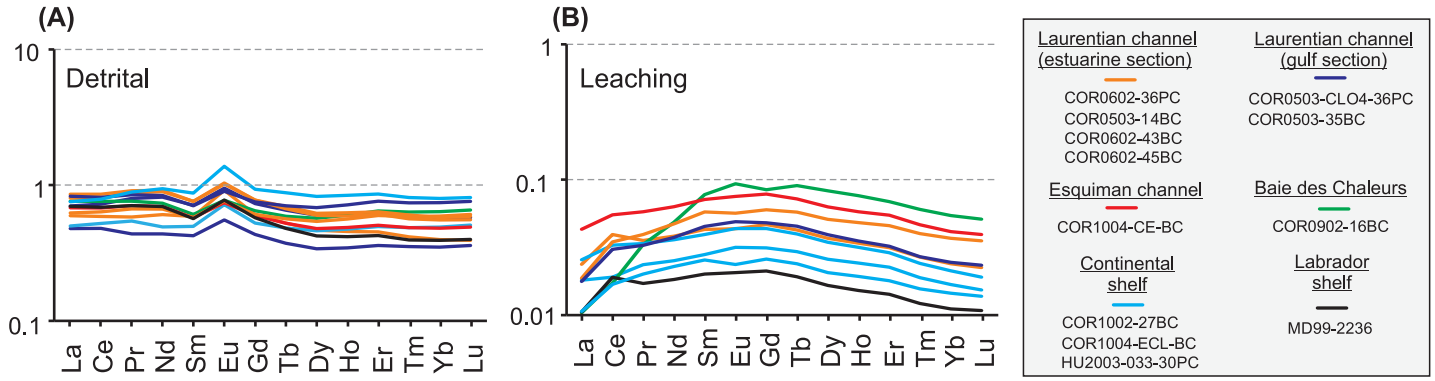

Figure 4

(Double column-full page width)

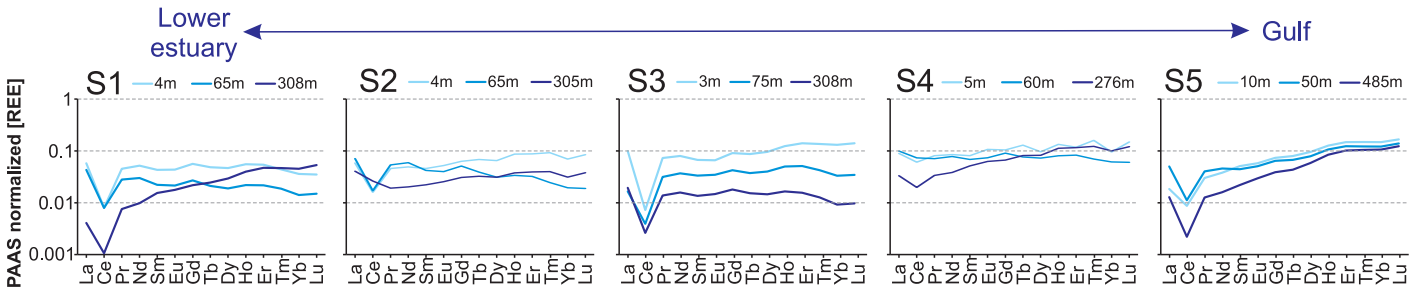

Figure 5

(Double column-full page width)

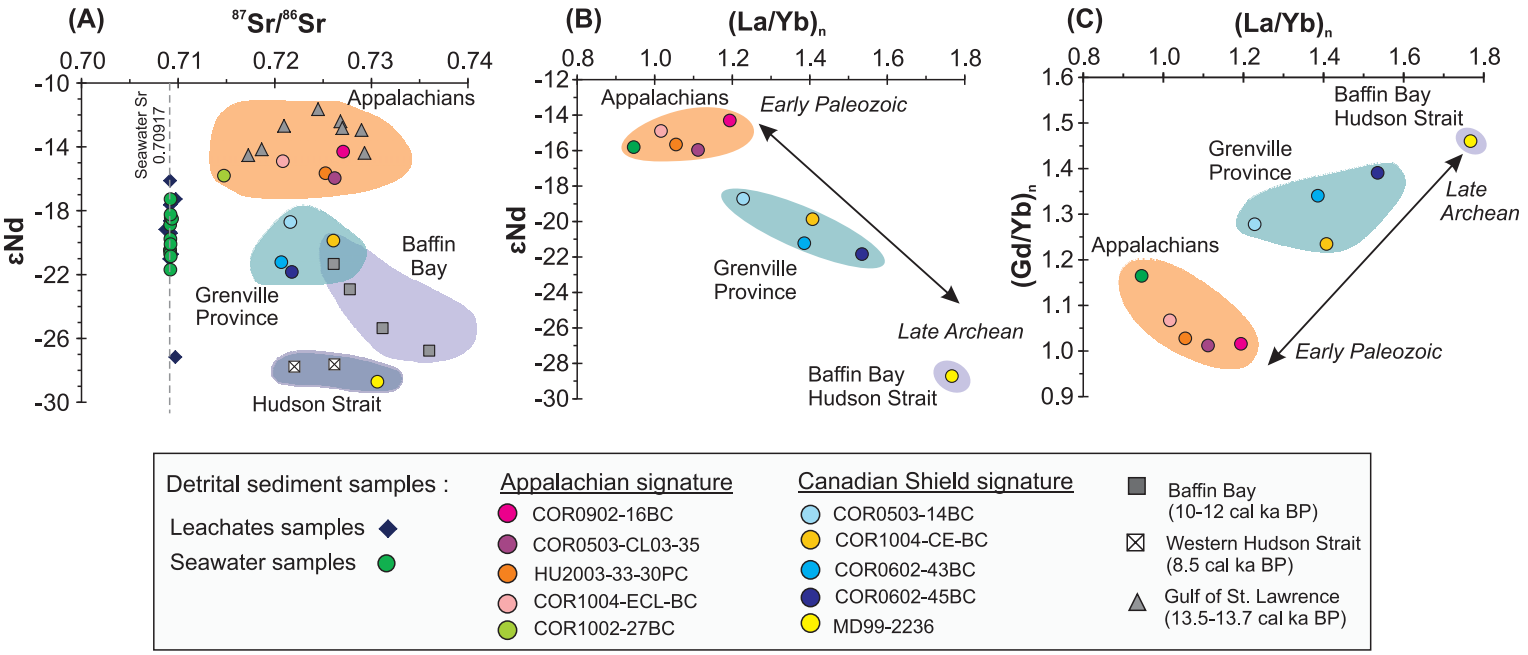

Figure 6

(Double column-full page width)

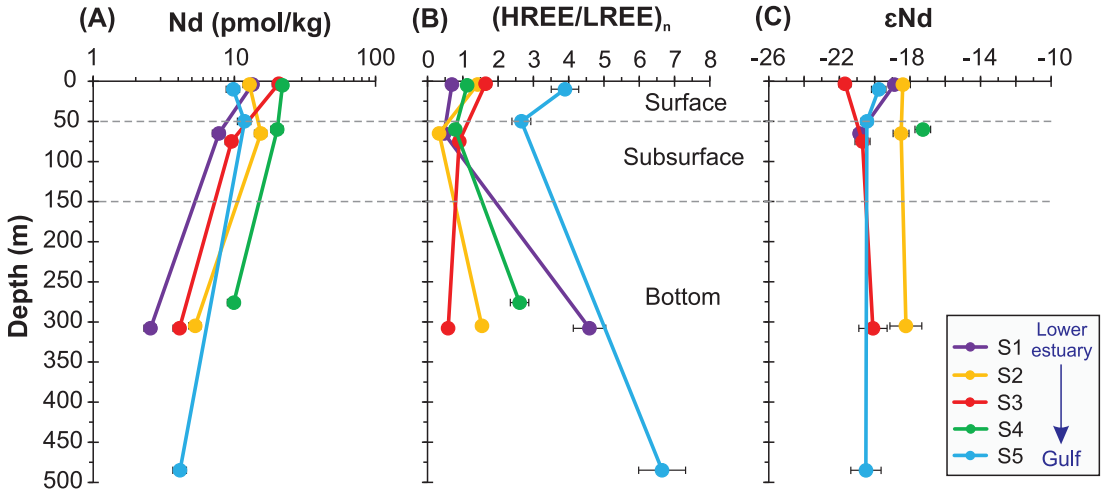

Figure 7

(Single column)

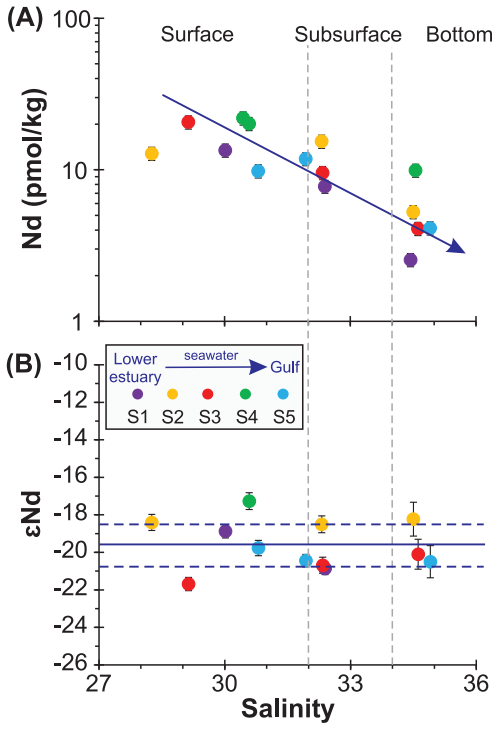

Figure 8

(Single column)

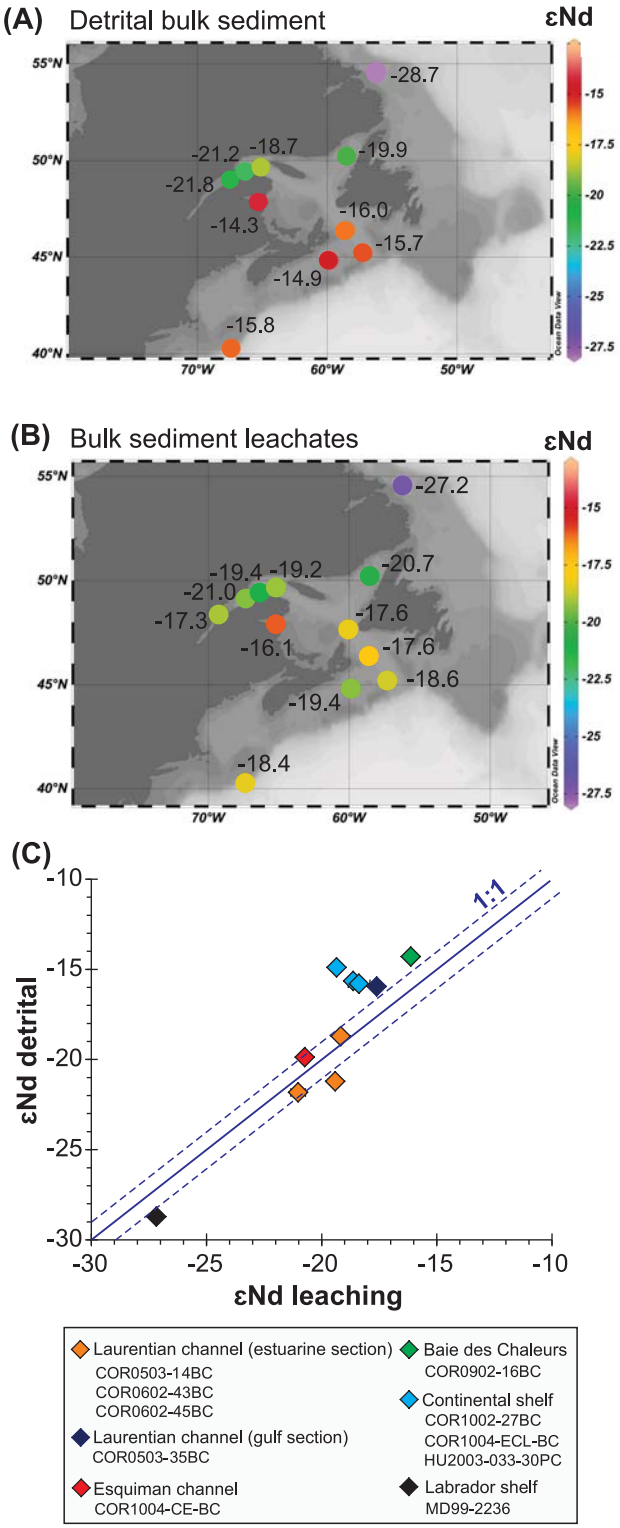

Figure 9

(Single column)

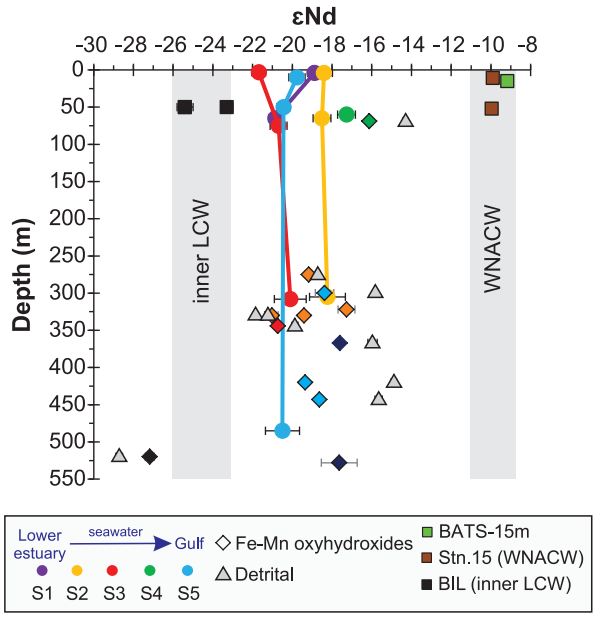

Figure 10

(Single column)

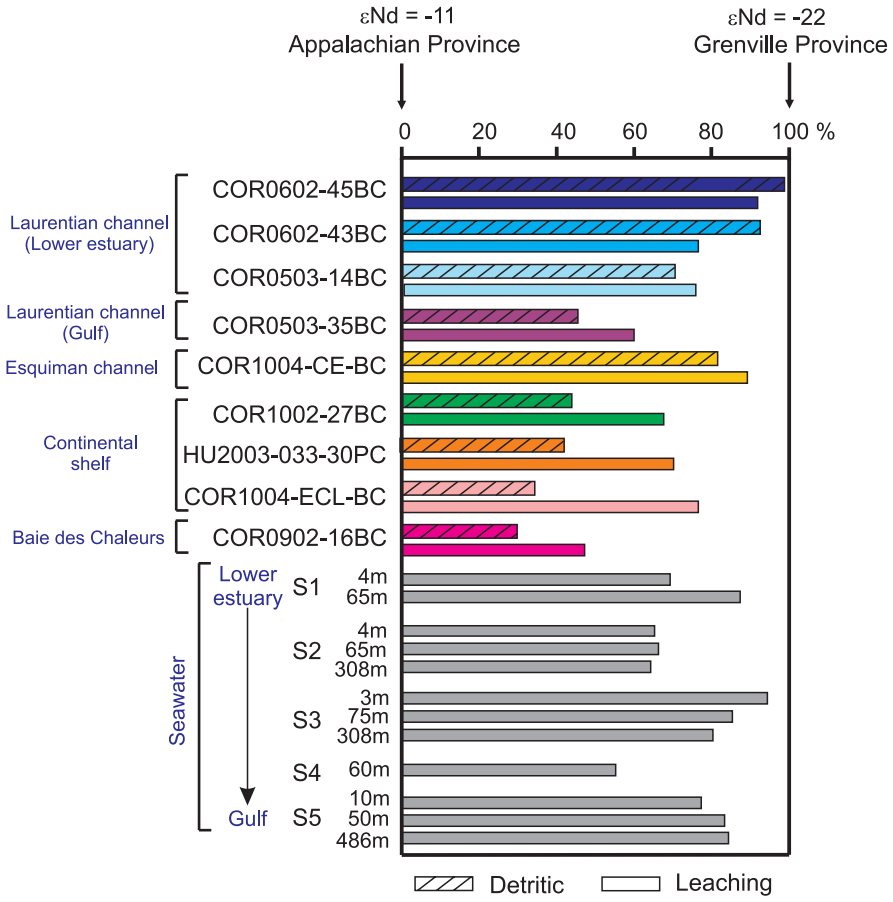

Figure 11

(Single column)

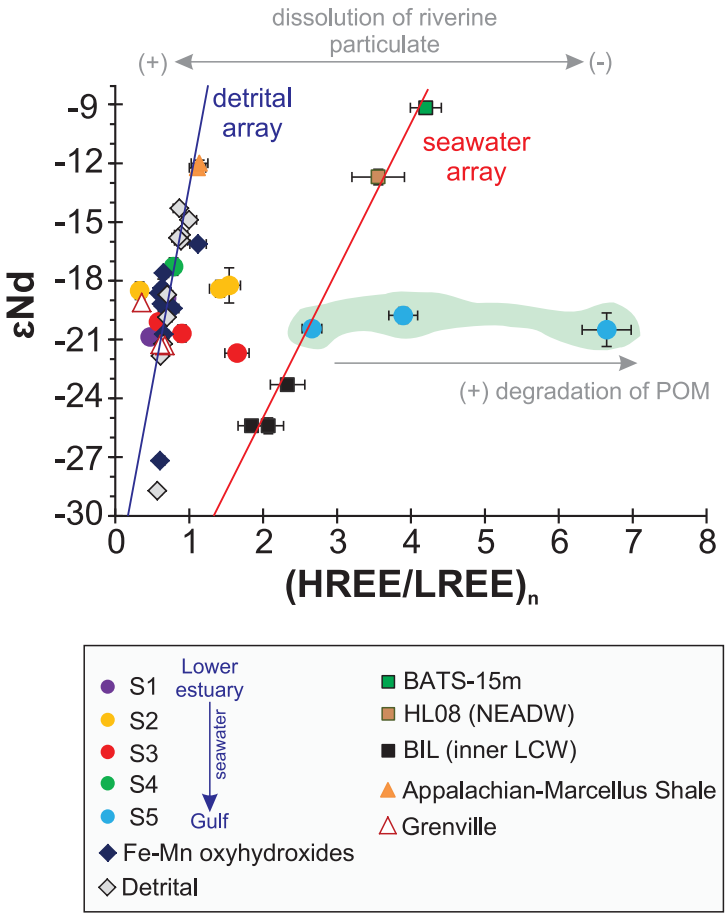

Figure S1

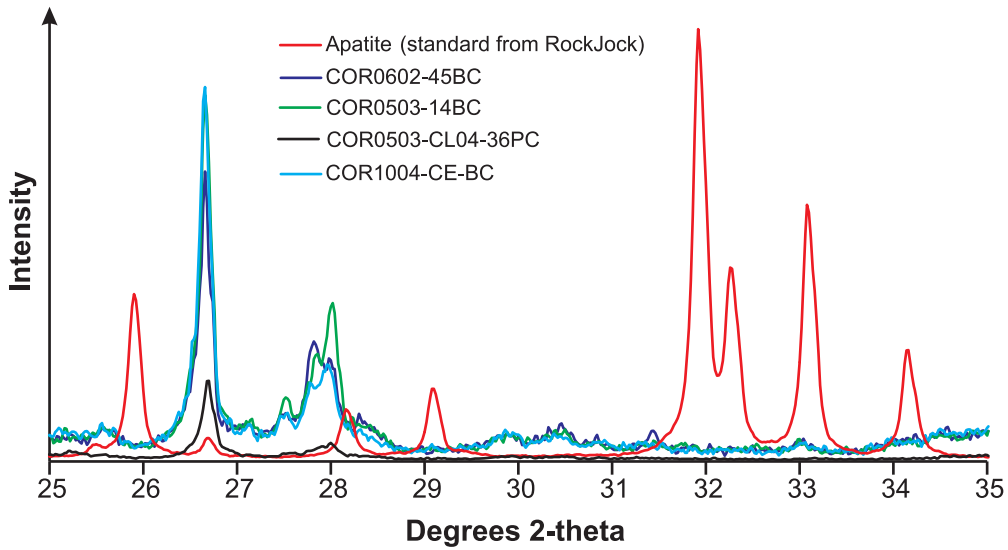
Apatite (standard from RockJock)
COR0602-45BC
COR0503-14BC
COR0503-CL04-36PC
COR1004-CE-BC
Intensity
25
26
27
28
29
30
31
32
33
34
35
Degrees 2-theta

Table S1. Location of core-top (0-1 cm) sediment samples with the corresponding water depth. Note that the box core (BC) sampler is designed for recovering a relatively undisturbed sample of the sediment-water interface. Likewise, the trigger weight corer (TWC) collected in conjunction with a piston corer (PC) also allows recovery of the sediment-water interface, which is usually perturbed when the piston corer enters the sediments. Thus, the core-top sediments sampled with the BC and TWC are assumed to have recovered the sediment-water interface, while this may not necessarily be the case with the PC. Core-top sediment samples represent <170 years (Smith and Schafer, 1999; Muzuka and Hillaire-Marcel, 1999; St-Onge et al., 2003; Barletta et al., 2010; Genovesi et al., 2011; Thibodeau et al., 2013), except for core MD99-2236 where the core-top represents around 425 years (Jennings et al., 2015).

Sample-ID	Sediment core sampler	Estimated core-top age (yr)	Latitude (DD)	Longitude (DD)	Depth (m)
COR1004-ECL-BC	BC	<100	44.8324	-59.8324	420
COR1002-27BC	BC	<100	40.2896	-67.3607	300
COR0503-35BC	BC	<100	46.4089	-58.5610	367
COR1004-CE-BC	BC	<170	50.2492	-58.5015	344
COR0503-14BC	BC	<100	49.6800	-65.1503	275
COR0602-45BC	BC	<100	49.4245	-66.3230	330
COR0602-43BC	BC	<100	49.1198	-67.2798	330
MD99-2236	PC	<425	54.6166	-56.1761	520
COR0902-16BC	BC	<100	47.9055	-65.2676	69
HU2003-033-30PC	TWC	<100	45.2125	-57.2163	443
COR0602-36PC	TWC	<100	48.4086	-69.3244	322
COR0503-CL04-36PC	TWC	<100	48.4611	-62.7194	528

Table S2. Location of estuarine water samples together with the hydrological parameters. The potential temperature (θ °C), salinity, potential density (σθ) and beam transmission (% light attenuation) obtained from the five estuarine water stations S1 (COR1206-030), S2 (COR1206-025), S3 (COR1207-003), S4 (COR1207-007) and S5 (COR1503-07) are indicated.

Stations	Latitude (DD)	Longitude (DD)	Depth (m)	θ (°C)	Salinity	σ_θ (kg.m^{-3})	Beam transmission (%)
S1	48.3987	-69.239	4	5.95	30.02	23.62	84.5
			65	1.29	32.39	25.93	98.2
			308	4.93	34.44	27.24	90.9
S2	48.6362	-68.635	4	8.06	28.26	21.98	82.9
			65	1.22	32.31	25.87	98.0
			308	5.06	34.45	27.27	92.5
S3	49.1835	-67.3517	3	8.44	29.14	22.61	93.9
			75	1.4	32.34	25.88	99.6
			308	5.32	34.61	27.33	92.3
S4	48.9695	-64.1403	5	6.78	30.44	23.86	96.8
			60	6.37	30.58	24.02	97.2
			276	5.37	34.56	27.28	91.0
S5	47.8784	-60.1748	10	5.91	30.80	24.30	97.4
			50	-0.26	31.93	25.88	97.5
			486	5.64	34.90	28.75	96.6

Table S3. Analytical results of REE concentrations (CLMS-1 in ng/mL and BHVO-2 in μg/g) in certified reference materials determined by ICP-Q-MS. QC: quality control; RD: relative deviation to reference values; RSD: relative standard deviation (1σ).

	QC CLMS-1				BHVO-2			
	QC1 (n=6)	RDS (%)	QC2 (n=7)	RDS (%)	This study	Reference values	RD	Accuracy (%)
La	1.25	10.6	4.0	3.6	15.6	15.2	1.0	103
Ce	1.25	11.4	4.0	3.8	37.3	37.5	1.0	99
Pr	1.25	10.4	4.0	2.8	4.9	5.3	0.9	91
Nd	1.25	10.9	4.0	3.1	22.3	24.3	0.9	92
Sm	1.25	10.2	4.0	2.3	5.5	6.0	0.9	92
Eu	1.25	10.3	4.0	2.8	1.9	2.0	0.9	91
Gd	1.25	10.2	4.0	3.0	5.7	6.2	0.9	92
Tb	1.25	10.5	4.0	2.2	0.8	0.9	0.9	89
Dy	1.25	10.4	4.0	1.8	4.6	5.3	0.9	87
Ho	1.25	10.6	4.0	2.2	0.9	1.0	0.9	87
Er	1.25	9.9	4.0	1.9	2.3	2.5	0.9	91
Tm	1.25	10.1	4.0	2.1	0.3	0.3	0.9	86
Yb	1.25	10.2	4.0	1.7	1.7	2.0	0.9	87
Lu	1.25	10.2	4.0	1.8	0.2	0.3	0.9	87

Table S4. REE concentrations (μg/g) for the detrital sediment samples. The HREE/LREE (Yb_n/Nd_n), (La/Yb)n, (Gd/Yb)n and Eu/Eu* ratios are also shown. The subscript "n" indicates PAAS-normalized abundances (Pourmand et al., 2012).

Sample-ID	La	Ce	Pr	Nd	Sm	Eu	Gd	Tb	Dy	Ho	Er	Tm	Yb	Lu	HREE/LREE (Yb_n/Nd_n)	(La/Yb)n	(Gd/Yb)n	Eu/Eu*
COR0602-36PC	26.04	50.89	5.80	22.18	3.97	1.08	3.61	0.46	2.44	0.47	1.37	0.19	1.18	0.17	0.66	1.49	1.53	1.52
COR0503-CL04-36PC	20.96	41.69	4.38	16.08	2.88	0.66	2.58	0.33	1.79	0.36	1.09	0.16	1.04	0.16	0.80	1.36	1.24	1.29
COR0503-14BC	30.65	62.44	7.91	29.72	4.79	1.13	4.33	0.57	3.12	0.62	1.88	0.26	1.69	0.25	0.70	1.23	1.28	1.31
COR1004-ECL-BC	21.88	45.27	5.42	18.08	3.36	0.85	3.12	0.42	2.42	0.49	1.50	0.22	1.46	0.22	1.00	1.02	1.07	1.40
COR0902-16BC	33.20	65.47	7.55	26.89	4.11	0.92	3.83	0.52	2.98	0.62	1.95	0.28	1.88	0.28	0.87	1.19	1.02	1.23
COR1004-CE-BC	29.73	58.57	7.02	25.33	3.89	0.88	3.54	0.46	2.51	0.51	1.53	0.22	1.43	0.21	0.70	1.41	1.23	1.26
MD99-2236	30.45	59.38	7.02	25.42	3.82	0.92	3.41	0.42	2.22	0.43	1.29	0.18	1.16	0.17	0.57	1.77	1.46	1.35
COR0602-45BC	37.25	73.79	9.00	33.28	5.10	1.20	4.58	0.58	3.13	0.61	1.84	0.25	1.64	0.24	0.61	1.53	1.39	1.32
HU2003-033-030PC	27.28	54.99	6.64	24.33	3.90	0.91	3.61	0.49	2.83	0.58	1.80	0.26	1.75	0.26	0.89	1.05	1.03	1.29
COR0602-43-BC	34.91	69.04	8.70	32.56	5.11	1.23	4.58	0.61	3.24	0.65	1.91	0.27	1.70	0.25	0.65	1.39	1.34	1.35
COR0503-CL03-35BC	36.00	70.11	8.41	30.56	4.74	1.07	4.45	0.62	3.55	0.74	2.29	0.33	2.19	0.33	0.89	1.11	1.01	1.24
COR1002-27BC	32.90	67.95	8.81	34.27	5.87	1.62	5.49	0.76	4.30	0.87	2.58	0.36	2.35	0.35	0.85	0.95	1.16	1.52

Table S5. REE concentrations (ng/g) for the bulk sediment leachate samples. The HREE/LREE (Yb_n/Nd_n) ratios are also shown. The subscript "n" indicates PAAS-normalized abundances (Pourmand et al., 2012).

Sample-ID	La	Ce	Pr	Nd	Sm	Eu	Gd	Tb	Dy	Ho	Er	Tm	Yb	Lu	HREE/LREE (Yb_n/Nd_n)
COR0503-14BC	1.05	3.47	0.36	1.43	0.30	0.05	0.28	0.04	0.20	0.04	0.10	0.01	0.07	0.01	0.63
COR1004-ECL-BC	0.80	1.68	0.24	0.94	0.19	0.04	0.19	0.03	0.14	0.03	0.07	0.01	0.05	0.01	0.67
COR0902-16BC	0.46	1.52	0.34	1.81	0.53	0.11	0.51	0.08	0.44	0.08	0.21	0.03	0.16	0.02	1.12
COR1004-CE-BC	1.91	4.85	0.59	2.35	0.49	0.09	0.47	0.06	0.33	0.06	0.17	0.02	0.12	0.02	0.65
MD99-2236	0.47	1.67	0.17	0.68	0.14	0.02	0.13	0.02	0.09	0.02	0.04	0.01	0.03	0.00	0.61
COR0602-45BC	0.04	0.09	0.01	1.76	0.02	0.00	0.02	0.01	0.06	0.02	0.08	0.01	0.09	0.01	0.66
HU2003-033-030PC	1.14	2.89	0.34	1.34	0.27	0.05	0.26	0.04	0.18	0.03	0.09	0.01	0.06	0.01	0.59
COR0602-43-BC	0.83	3.05	0.40	1.76	0.40	0.07	0.36	0.05	0.27	0.05	0.14	0.02	0.11	0.02	0.78
COR0503-CL03-35BC	0.79	2.69	0.33	1.40	0.31	0.06	0.29	0.04	0.21	0.04	0.10	0.01	0.07	0.01	0.65
COR1002-27BC	0.47	1.49	0.20	0.85	0.18	0.03	0.16	0.02	0.11	0.02	0.06	0.01	0.04	0.01	0.63

Table S6. REE concentrations from the five seawater stations (pmol/kg). The HREE/LREE (Yb_n/Nd_n) ratios are also shown. The subscript "n" indicates PAAS-normalized abundances (Pourmand et al., 2012).

Stations	Depth(m)	La	Ce	Pr	Nd	Sm	Eu	Gd	Tb	Dy	Ho	Er	Tm	Yb	Lu	HREE/LREE (Yb_n/Nd_n)
S1	4	18.53	5.05	3.26	13.43	1.98	0.35	2.17	0.27	1.53	0.35	0.99	0.12	0.62	0.09	3.9
S1	65	13.85	4.99	2.02	7.76	1.02	0.17	1.03	0.12	0.62	0.14	0.40	0.05	0.25	0.04	2.7
S1	308	1.31	0.67	0.55	2.54	0.71	0.14	0.84	0.14	0.96	0.25	0.87	0.12	0.79	0.13	6.6
S2	4	18.85	10.10	3.31	12.80	2.10	0.42	2.44	0.39	2.14	0.56	1.62	0.25	1.22	0.21	1.6
S2	65	22.94	10.79	3.89	15.40	1.93	0.32	1.97	0.22	1.03	0.22	0.59	0.07	0.34	0.05	0.9
S2	305	13.06	16.60	1.39	5.27	1.02	0.20	1.19	0.18	1.02	0.24	0.73	0.11	0.55	0.10	0.6
S3	3	31.83	4.57	5.27	20.64	3.06	0.53	3.49	0.49	3.13	0.79	2.59	0.36	2.29	0.35	0.7
S3	75	5.30	2.47	2.27	9.55	1.53	0.28	1.63	0.21	1.31	0.32	0.94	0.11	0.58	0.09	0.5
S3	308	6.24	1.65	0.99	4.09	0.62	0.12	0.69	0.09	0.48	0.11	0.29	0.03	0.16	0.02	4.6
S4	5	28.54	38.08	5.81	21.92	3.68	0.85	4.00	0.72	3.14	0.85	2.16	0.42	1.66	0.37	1.1
S4	60	31.75	46.14	5.09	20.13	3.12	0.59	3.48	0.43	2.38	0.51	1.52	0.19	1.06	0.15	0.8
S4	276	10.60	12.43	2.42	9.91	2.34	0.50	2.54	0.45	2.69	0.71	2.12	0.33	1.74	0.30	2.6
S5	10	5.91	5.49	2.16	9.81	2.32	0.46	2.81	0.45	3.12	0.81	2.72	0.39	2.57	0.42	1.4
S5	50	16.04	7.03	2.90	11.80	2.03	0.41	2.47	0.38	2.58	0.68	2.26	0.33	2.11	0.35	0.3
S5	485	4.11	1.38	0.91	4.12	1.01	0.24	1.49	0.24	1.92	0.54	1.87	0.28	1.84	0.31	1.5

Table S7. Neodymium (Nd) and strontium (Sr) isotope compositions obtained for the five estuarine water stations, bulk sediment leachates and detrital sediments. Note that the five water stations COR1206-030, COR1206-025, COR1207-003, COR1207-007 and COR1503-007 studied here are referred to as S1, S2, S3, S4, and S5, respectively. The symbols * and + indicate replicate analysis and NA indicate sample not analyzed.

Sample-ID	$^{143}Nd/^{144}Nd$	2σ	εNd	2σ	$^{87}Sr/^{86}Sr$	2σ
Estuarine waters						
S1-4m	0.51167	0.00002	-18.0	0.4	0.70918	0.00009
S1-65m	0.51157	0.00002	-20.9	0.3	0.70925	0.00008
S1-308m	NA	NA	NA	NA	NA	NA
S2-4m	0.51169	0.00002	-18.4	0.4	0.70923	0.00007
S2-65m	0.51169	0.00002	-18.5	0.4	0.70937	0.00012
S2-308m	0.5117	0.00005	-18.2	0.9	0.70921	0.00005
S3-3m	0.51153	0.00002	-21.7	0.4	0.7092	0.00007
S3-75m	0.51158	0.00002	-20.7	0.4	0.70918	0.00004
S3-308m	0.51161	0.00004	-20.1	0.8	0.70921	0.00006
S4-5m	NA	NA	NA	NA	0.70928	0.00006
S4-60m	0.51175	0.00002	-17.3	0.4	0.70922	0.00002
S4-276m	NA	NA	NA	NA	0.70926	0.00006
S5-10m	0.51162	0.00002	-19.8	0.4	0.70921	0.00004
S5-50m	0.51159	0.00002	-20.4	0.3	0.70915	0.00008
S5-485m	0.51159	0.00004	-20.5	0.9	0.70918	0.00011
Fe-Mn oxyhydroxides						
COR0902-16BC	0.51181	0.00001	-16.1	0.2	0.70918	0.00002
COR0503-CL03-35BC	0.51174	0.00001	-17.6	0.2	0.70925	0.00003
2003-033-030PC	0.51168	0.00001	-18.6	0.2	0.70917	0.00002
COR0503-CL04-36PC	0.51173	0.00005	-17.6	0.9	0.70916	0.00004
COR-0602-043-BC	0.51164	0.00001	-19.4	0.2	0.70925	0.00003
COR0602-045BC	0.51156	0.00002	-21.0	0.3	0.70910	0.00005
COR0602-36PC	0.51175	0.00002	-17.3	0.4	0.70975	0.00004
COR0503-14BC	0.51166	0.00001	-19.2	0.2	0.70870	0.00002
COR1004-ECL-BC	0.51165	0.00001	-19.4	0.2	0.70920	0.00002
COR1002-27BC	0.51170	0.00002	-18.4	0.4	0.70930	0.00002
COR1004-CE-BC	0.51158	0.00001	-20.7	0.2	0.70938	0.00001
MD99-2236	0.51124	0.00001	-27.2	0.2	0.70973	0.00001
*COR0602-36PC-IJ-5-6cm_A	0.51175	0.00002	-17.3	0.4	NA	NA
*COR0602-36PC-IJ-5-6cm_B	0.51169	0.00003	-18.4	0.6	NA	NA
*COR0602-36PC-IJ-5-6cm_C	0.51170	0.00002	-18.3	0.4	NA	NA
+COR0503-CL04-36PC-KL-27-28cm_A	0.51173	0.00005	-17.6	0.5	NA	NA
+COR0503-CL04-36PC-KL-27-28cm_B	0.51175	0.00001	-17.4	0.2	NA	NA
Detrital						
COR0902-16BC	0.51190	0.00001	-14.3	0.1	0.72708	0.00001
COR0503-CL03-35BC	0.51182	0.00001	-16.0	0.2	0.72621	0.00002
2003-033-030PC	0.51184	0.00001	-15.7	0.2	0.72525	0.00003
COR0602-043-BC	0.51155	0.00001	-21.2	0.2	0.72068	0.00002
COR0602-045BC	0.51152	0.00001	-21.8	0.1	0.72178	0.00002
COR0503-14BC	0.51168	0.00001	-18.7	0.1	0.72160	0.00001
COR1004-ECL-BC	0.51187	0.00001	-14.9	0.1	0.72083	0.00002
COR1002-27BC	0.51183	0.00001	-15.8	0.1	0.71475	0.00002
COR1004-CE-BC	0.51162	0.00001	-19.9	0.2	0.72607	0.00001
MD99-2236	0.51117	0.00001	-28.7	0.2	0.73062	0.00002

REE distribution and Nd isotope composition of estuarine waters and bulk sediment leachates tracing lithogenic inputs in eastern Canada

Marie Casse, Jean-Carlos Montero-Serrano, Guillaume St-Onge, André Poirier

Supplementary material

Analytical procedures

Seawater treatment

The pre-concentration of REEs of estuarine water was analyzed following the analytical procedures outlined in Shabani et al. (1992) and Jeandel et al. (1998) and used in other oceanographic studies that address REE concentrations in seawater (e.g., Zhang and Nozaki, 1996; Lacan and Jeandel, 2001; Copard et al., 2011; Wu et al., 2015). Briefly, after the pH of the water samples had been raised to 3.5 using an ammonia solution (NH4OH; 25%, Merck Suprapur®), REEs were preconcentrated by pumping water samples through the a SEP-PAK Classic C18 cartridge loaded with a strong REE complexant [HDEHP/H_2MEHP; di(2-ethyl)hydrogen-phosphate and 2-ethylhexyldihydrogen-phosphate; Shabani et al., 1992]. In order to destroy organic components, the pre-concentrated REEs were then treated with 4.5 mL of aqua regia for at least 24 h at 110°C and subsequently evaporated. Samples were re-dissolved in 2 mL 7M HNO_3, and the solutions were divided into two aliquots of 1 mL for REE concentration and Nd-Sr separation, respectively. The aliquot for REE concentration analysis was evaporated to dryness and re-dissolved in 1 mL of concentrated HNO_3 and subsequently diluted with Milli-Q water to a total volume of 5 mL. The aliquot for the Sr-Nd separation was evaporated to dryness and re-dissolved in 2 mL of 2.5 M HCl before ion exchange chemistry.

Bulk sediment leaching

Nd and Sr isotope signatures from authigenic Fe-Mn coatings of the bulk sediment were extracted applying the leaching protocol of Chen et al. (2012). Briefly, 200 mg of dried and powdered sediment were rinsed three times with Milli-Q water. Next, Sr and Nd contained in the sediment oxyhydroxide fraction were leached for about 30 min in a single step using a dilute reducing and complexing solution consisting of 0.005M hydroxylamine hydrochloride (HH), 1.5% acetic acid, and 0.03M Na-EDTA, buffered to pH 4 with suprapur NaOH. A buffered acetic acid leach step was omitted since biogenic carbonates are negligible in all sediment samples (Casse et al., 2017). During treatment, the sediment samples were gently shaken to enhance the reaction. After centrifugation, the leach solution was decanted, evaporated, and re-dissolved in 2 mL of 2.5 M HCl. This last solution was divided into two aliquots of 1 mL, one for the REE concentration analyses and the other one for the Nd and Sr chromatographic extraction. The aliquot for REE concentration analysis was evaporated to dryness and re-dissolved in 1 mL of concentrated HNO_3 and subsequently diluted with Milli-Q water to a total volume of 5 mL.

Bulk sediment digestion (detrital fraction)

In order to assess the different sources of the detrital particles, the previously leached sediments were leached again for about 24 h with a stronger leaching solution (0.05 M HH) to ensure complete removal of residual Fe-Mn oxyhydroxides. Next, leached sediment samples were digested using a hydrofluoric-nitric-perchloric ($HF\text{-}HNO_3\text{-}HClO_4$) procedure modified from Révillon and Hureau-Mazaudier (2009). Briefly, approximately 200 mg of powder sediment samples were weighed into 100 mL microwave PTFE vessels. A mixture of concentrated $HNO_3/HF/HCLO_4$ (1:6:1 mL; Optima™ grade) was added to dissolve aluminosilicates. Samples were run in a microwave for 10 min at 175°C and 30 min at 220°C.

Samples were left to cool and transferred to 30 ml Savillex® PFA Teflon® beakers. To minimize sample loss by adsorption onto the microwave vessels, the interior of each vial was rinsed with about 2 mL of concentrated HNO_3. Beakers were heated at 120°C to reduce solution volume to incipient desiccation. Subsequently, 1 mL of concentrated HNO_3 and 4 mL of concentrated H_2O_2 (Optima™ grade) were added to remove remaining organic matter from the solution. Samples were dried once more at 120°C and re-dissolved in 3 mL of 6M HCl. This solution was again dried at 120°C. Samples were finally re-dissolved in 2.2 mL of 2.5M HCl. The solution was divided into two aliquots of 1 mL, one for the REE concentration analyses and the other one for the Nd and Sr chromatographic extraction. The aliquot for REE concentration analysis was evaporated to dryness and re-dissolved in 1 mL of concentrated HNO_3 and subsequently diluted with Milli-Q water to a total volume of 5 mL.

Column chemistry: Sr and Nd separation

Sr and Nd are separated from other elements applying a single-step ion chromatographic separation (Li et al., 2014). Briefly, solutions obtained from previous steps (seawater, leaching, and detrital fraction) were centrifuged at 5000 rpm for 8 min. Then, 1 mL of the supernatant solution was passed through a two-layered mixed resin column (70 mm length, 6 mm diameter) with the upper layer containing 1.5 mL of Biorad® AG50W-X12 (200–400 mesh) resin and the bottom layer containing 0.45 mL of Eichrom® LN Spec resin (100–150 μm). Before sample loading for separation of Sr–Nd from the sample matrix, the mixed resin column was pre-washed with 18 mL of 6 M HCl, 8 mL of 3 M HF, and 4 mL of H2O in turn. After sample loading and rinsing four times with 0.5 mL of 2.5 M HCl, the column was washed with 13.5 mL of 2.5 M HCl. Most matrix elements (K, Ca, Na, Mg, Al, Fe, Mn, Ti) and Rb were removed during this step. Then, the Sr fraction was stripped with 5.5 mL of 2.5 M HCl. Some of the HREEs (Dy, Ho, Er, Tm, Yb, Lu) and Ba were then washed out with 3 mL of 2.5 M HCl. Next, Nd was

then isolated from other REEs with 8 mL of 6 M HCl. Sr and Nd fractions were heated on a hotplate at 120°C to dryness and prepared for isotope measurements.

REE concentrations and Sr-Nd analysis

REE concentrations are determined using an inductively coupled plasma-quadrupole mass spectrometer (ICP-QMS Agilent 7500c) at the *Institut des sciences de la mer de Rimouski* (ISMER, Canada). Polyatomic oxide and hydroxide interferences for the REE were corrected using oxide formation rates determined from the periodic measurement of Milli-Q water and single element standard solutions (4 ng/mL for each element) of Ba, Ce, Pr + Nd, and Sm + Eu + Gd + Tb, following the procedure of Barrat et al. (1996) and Smirnova et al. (2003). Procedural blanks for REE (chemistry and mass spectrometry) always account for less than 1% of the lowest concentration measured in the samples. Note that no international seawater standards (such as BATS and NASS-7) were measured in this study. Instead, a multi-element stock standard solution containing all REE (multi-element solution 1, CLMS-1, Spex Certiprep Inc., Quebec, Canada) was used to prepare external calibration and quality control (QC) solutions. The seven calibration concentrations ranged from 20.0 to 0.31 ng/mL and QC concentrations were 1.25 and 4 ng/mL of REE. ICP-QMS reproducibility, based on replicate analysis of these QC solutions every 15 samples, was <11% relative standard deviation (RSD, 1σ) for all REEs (**Table S3**). The accuracy of the overall method including the detrital digestion was assesses by analyzing the USGS rock standard BHVO-2 (basalt). The results obtained for this reference material are in good agreement with reference values from the GeoREM database (http://georem.mpch-mainz.gwdg.de/). Overall, compositions only deviate from reference values by <14% (**Table S3**).

REE are normalized to Post Archaean Australian Shale (PAAS, Pourmand et al., 2012). Thus, the subscript “n” indicates PAAS-normalized abundances. Based on several geochemical studies that

address REE concentrations in authigenic phases and seawaters (Haley et al., 2004; Molina-Kescher et al., 2014; Osborne et al., 2015; Laukert et al., 2017), we used the indices HREE/LREE ([Yb]n/[Nd]n) to investigate the fractionation between HREE and LREE. In the detrital fraction, HREE versus LREE enrichment is quantified by (La/Yb)n, HREE versus MREE is quantified by (Gd/Yb)n, and Eu-anomaly is quantified as follows: $Eu/Eu^* = 3Eu_n/(2*Sm_n + Tb_n)$ (e.g., Armstrong-Altrin et al., 2013, 2016).

Sr isotope ratios ($^{88}Sr/^{86}Sr$) were measured in dynamic mode on a Thermo Scientific Triton Plus™ multicollector thermal ionization mass spectrometer (TIMS) at GEOTOP (Montreal, Canada). Sr samples were loaded and analyzed on a single Re center filament. The mass bias is corrected using a $^{86}Sr/^{88}Sr$ ratio of 0.1194, assuming exponential fractionation behavior. Repeated analyses of the NIST-987 standard (n=5) yield values of 0.71026 (± 0.00001, 2σ reproducibility). This mean value compares well to its certified value of 0.71025 ± 0.00001 (Weis et al., 2006)**.** The total procedural blanks for Sr was less than 0.5 ng which is considered negligible compared to the sample yields (>100 ng).

Nd isotope ratios ($^{146}Nd/^{144}Nd$) are analyzed on a Nu Instruments Multi-Collector Inductively Coupled Plasma Mass Spectrometer (MC-ICP-MS), also at GEOTOP. The mass-bias correction is performed by normalizing $^{146}Nd/^{144}Nd$ to 0.7219 and applying an exponential-fractionation correction. Replicate analyses of the standard JNdi-1 yielded a mean value of $^{143}Nd/^{144}Nd = 0.512108 \pm 0.000020$ (2σ; n=20) which is within the uncertainty of its certified value of 0.512115 ±0.000007 (Tanaka et al., 2000). Hence, no correction has been applied to the Nd isotope data. The external reproducibility of MC-ICP-MS measurements of Nd isotope standard JNdi-1, at the same concentration as the samples, ranged from 0.2 to 0.4 ε units (2σ; n=31) for various analytical sessions. Thus, the analytical error associated to each sample analysis is taken as the external reproducibility of the JNdi-1 standard for each session. However, measurement uncertainties for some samples are higher (up to 0.9 ε units; Table S5) than those of the Nd standards, because of poorer counting statistics of samples with low Nd concentration

(mainly in water samples). The total procedural blanks for Nd were <100 pg, and were therefore neglected as they represented less than 0.2% of the Nd content of the most depleted sample analyzed from seawater, leachates, and detrital sediments. Nd isotope ratios are expressed as follows: εNd = ([($^{143}Nd/^{144}Nd)_{sample}$/($^{143}Nd/^{144}Nd)_{CHUR}$]-1)x10000 (CHUR: Chrondritic Uniform Reservoir; Jacobsen and Wasserburg, 1980).

References

Armstrong-Altrin, J.S., Nagarajan, R., Madhavaraju, J., Rosalez-Hoz, L., Lee, Y.I., Balaram, V., Cruz-Martínez, A., & Avila-Ramírez, G. (2013). Geochemistry of the Jurassic and Upper Cretaceous shales from the Molango Region, Hidalgo, eastern Mexico: Implications for source-area weathering, provenance, and tectonic setting. Comptes Rendus Geoscience, 345(4), 185–202.

Armstrong-Altrin, J.S., Lee, Y.I., Kasper-Zubillaga, J.J., & Trejo-Ramírez, E. (2016). Mineralogy and geochemistry of sands along the Manzanillo and El Carrizal beach areas, southern Mexico: implications for palaeoweathering, provenance and tectonic setting: Geochemistry of Beach Sands from Southern Mexico. Geological Journal, 57, 1446–1461.

Barrat, J.-A., Keller, F., Amosse´, J., Taylor, R.N., Nesbitt, R.W., Hirata, T. (1996). Determination of rare earth elements in sixteen silicate reference samples by ICP-MS after Tm addition and ion exchange separation. Geostand. Newsl. 20, 133– 139.

Casse, M., Montero-Serrano, J.-C., & St-Onge, G. (2017). Influence of the Laurentide Ice Sheet and relative sea-level changes on sediment dynamics in the Estuary and Gulf of St. Lawrence since the last deglaciation, Boreas. doi:10.1111/bor.12230

Chen, T.-Y., Frank, M., Haley, B.A., Gutjahr, M., & Spielhagen, R.F. (2012). Variations of North Atlantic inflow to the central Arctic Ocean over the last 14 million years inferred from hafnium

and neodymium isotopes. Earth and Planetary Science Letters, 353, 82–92. doi:10.1016/j.epsl.2012.08.012

Copard, K., Colin, C., Frank, N., Jeandel, C., Montero Serrano, J.-C., Reverdin, G., Ferron, B., 2011. Nd isotopic composition of water masses and dilution of the Mediterranean outflow along the South-West European margin. Geochem. Geophys. Geosyst. 12, Q06020, http://dx.doi.org/10.1029/2011GC003529.

Haley, B. A., Klinkhammer, G. P., & McManus, J. (2004). Rare earth elements in pore waters of marine sediments. Geochimica et Cosmochimica Acta, 68(6), 1265–1279.

Jacobsen, S. B., & Wasserburg, G. J. (1980). Sm-Nd isotopic evolution of chondrites. Earth and Planetary Science Letters, 50(1), 139–155.

Jeandel, C., Thouron, D., & Fieux, M. (1998). Concentrations and isotopic compositions of neodymium in the eastern Indian Ocean and Indonesian straits. Geochimica et Cosmochimica Acta, 62(15), 2597–2607.

Lacan, F. & Jeandel, C. (2001). Tracing Papua New Guinea imprint on the central Equatorial Pacific Ocean using neodymium isotopic compositions and Rare Earth Element patterns. Earth and Planetary Science Letters, 186(3), 497–512. doi:10.1016/S0012-821X(01)00263-1

Laukert, G., Frank, M., Bauch, D., Hathorne, E. C., Gutjahr, M., Janout, M., et al. (2017).Transport and transformation of riverine neodymium isotope and rare earth element signatures in high latitude estuaries: a case study from the Laptev Sea. Earth Planet. Sci. Lett. 477, 205–217.

Li, C.-F., Guo, J.-H., Yang, Y.-H., Chu, Z.-Y., & Wang, X.-C. (2014). Single-step separation scheme and high-precision isotopic ratios analysis of Sr–Nd–Hf in silicate materials. Journal of Analytical Atomic Spectrometry, 29(8), 1467.

Molina-Kescher, M., Frank, M., & Hathorne, E. C. (2014). Nd and Sr isotope compositions of different phases of surface sediments in the South Pacific: Extraction of seawater signatures, boundary exchange, and detrital/dust provenance. Geochemistry, Geophysics, Geosystems, 15(9), 3502–3520.

Osborne, A.H., Haley, B.A., Hathorne, E.C., Plancherel, Y., & Frank, M. (2015). Rare earth element distribution in Caribbean seawater: Continental inputs versus lateral transport of distinct REE compositions in subsurface water masses. Marine Chemistry 177, 172–183.

Pourmand, A., Dauphas, N., & Ireland, T.J. (2012). A novel extraction chromatography and MC-ICP-MS technique for rapid analysis of REE, Sc and Y: Revising CI-chondrite and Post-Archean Australian Shale (PAAS) abundances. Chemical Geology 291, 38–54.

Révillon, S., and D. Hureau-Mazaudier, 2009. Improvements in digestion protocols for trace element and isotope determinations in stream and lake sediment reference materials (JSd-1, JSd-2, JSd-3, JLk-1 and LKSD-1). Geostandards & Geoanalytical Research 33, 397-413.

Shabani, M. B., Akagi, T., & Masuda, A. (1992). Preconcentration of trace rare-earth elements in seawater by complexation with bis (2-ethylhexyl) hydrogen phosphate and 2-ethylhexyl dihydrogen phosphate adsorbed on a C18 cartridge and determination by inductively coupled plasma mass spectrometry. Analytical Chemistry, 64(7), 737–743.

Smirnova, E.V., Fedorova, I.N., Sandimirova, G.P., Petrov, L.L., Balbekina, N.G., Lozhkin, V.I., 2003. Determination of rare earth elements in black shales by inductively coupled plasma mass spectrometry. Spectrochim. Acta B: Atomic Spectroscopy 58, 329-340.

Tanaka, T., Togashi, S., Kamioka, H., Amakawa, H., Kagami, H., Hamamoto, T., Yuhara, M., Orihashi, Y., Yoneda, S., Shimizu, H., Kunimaru, T., Takahashi, K., Yanagi, T., Nakano, T., Fujimaki, H.,

Shinjo, R., Asahara, Y., Tanimizu, M., & Dragusanu, C. (2000). JNdi-1: a neodymium isotopic reference in consistency with LaJolla neodymium. Chemical Geology, 168(3), 279–281.

Weis, D., Kieffer, B., Maerschalk, C., Barling, J., de Jong, J., Williams, G.A., Hanano, D., Pretorius, W., Mattielli, N., Scoates, J.S., Goolaerts, A., Friedman, R.M., & Mahoney, J.B. (2006). High-precision isotopic characterization of USGS reference materials by TIMS and MC-ICP-MS: isotopic study of USGS reference materials. Geochemistry, Geophysics, Geosystems 7(8). doi:10.1029/2006GC001283

Wu, Q., Colin, C., Liu, Z., Thil, F., Dubois-Dauphin, Q., Frank, N., Tachikawa, K., Bordier, L., & Douville, E. (2015). Neodymium isotopic composition in foraminifera and authigenic phases of the South China Sea sediments: Implications for the hydrology of the North Pacific Ocean over the past 25 kyr: hydrology of the North Pacific Ocean. Geochemistry, Geophysics, Geosystems, 16(11), 3883–3904. doi:10.1002/2015GC005871

Zhang J. and Nozaki Y. (1996). Rare earth elements and yttrium in seawater: ICP-MS determinations in the East Caroline, Coral Sea, and South Fiji basins of the western South Pacific Ocean. Geochimica et Cosmochimica Acta 60, 4631–4644.